Thermal and mechanical studies of carbon nanotube-polymer composites synthesized at high pressure and high temperature

Bounphanh Tonpheng

Doctoral Thesis
Department of physics
University of Umeå, Sweden
Umeå, 2011

Thermal and mechanical studies of carbon nanotube-polymer composites synthesized at high pressure and high temperature

Umeå University
SE-901 87 Umeå
Sweden

ISBN: 978-91-7459-223-8

Printed by Print&Media, Umeå 2011

To my family

Abstract

In this thesis, thermal and mechanical properties of polymers and carbon nanotubes-polymer composites, which were modified and studied under high pressure, are presented. The results concern the thermal conductivity κ and heat capacity per unit volume ρc_p of pure polymers: polyisoprene (PI), polybutadiene (PB), and nylon-6, and their multi-wall and single-wall carbon nanotube (MWCNT and SWCNT) composites both before (untreated) and after high pressure treatments. As shown here, a suitable high pressure high temperature (HP&HT) treatment induces either cross-links in the polymers (PI and PB), i.e. transforms these into elastomers, or increases the crystallinity (nylon-6).

The experiments were done, in situ, in the temperature range 100-520 K for pressures up to 1.5 GPa, and the results show that cross-linking under high pressure can be monitored in data for κ and ρc_p. Moreover, κ for a well cross-linked (ebonite-like) polymer near ambient conditions can be up to 50% higher than the untreated states, whereas ρc_p becomes similar as the glassy state of the untreated polymer. The glass transition of the cross-linked states becomes broader and shifts to higher temperatures with increasing degree of cross-linking. In the case of nylon-6, the HP&HT treatment causes microstructural changes, viz. increased crystallinity and crystals with a preferred orientation and increased size, which enhances κ and improves the thermal stability.

The thermal property studies of the CNT polymer composite show that κ of the composites increases significantly, e.g. 120% for 5wt% SWCNTs in PI, which is attributed to the very high κ of CNTs. Moreover, MWCNTs also improve κ, but not as much as SWCNTs. This is accounted for by their lower aspect ratio (length/diameter), whereas their lower κ is less important. Adding CNTs normally raise the glass transition temperatures of the polymers. More specifically, SWCNTs in PB raise the glass transition temperature slightly more than MWCNTs and, in particular, under the most densified conditions and for a high molecular weight PB, which may be due to more favorable conditions for coating/wrapping of the CNTs.

The mechanical studies of the HP&HT treated polymers and composites show that CNTs strongly enhances the tensile strength and Young's modulus, e.g. 5 wt% SWCNT in PI synthesized at 1 GPa and 513 K showed 2 times higher tensile strength and 2.3 times higher Young's modulus than that of similarly treated pure PI. The results indicate that the treatment improves the poor interfacial contact between the CNTs and polymer, which is one of the obstacles for achieving stronger CNT composites.

Keywords: polymer, carbon nanotubes, pressure, heat capacity, Young's modulus, cross-link density.

Sammanfatting

I denna avhandling presenteras termiska och mekaniska egenskaper för polymerer och polymera kolnanorörs kompositer som behandlats och undersökts under höga tryck och höga temperaturer. Resultaten omfattar värmeledningsförmågan κ och värmekapaciteten per volymenhet ρc_p för rena polymerer: polyisopren (PI), polybutadien (PB) och nylon-6 och deras flerväggiga och enväggiga kolnanorörs (MWCNTs och SWCNTs) kompositer både före (obehandlat) och efter högtrycksbehandlingar. Studien visar att en lämplig behandling vid högt tryck och hög temperatur (HP&HT) inducerar antingen tvärbindningar i polymeren (PI och PB), dvs förvandlar dessa till elastomerer, eller så ökar kristalliniteten (nylon-6).

Försöken gjordes, in situ, i temperaturområdet 100-520 K för tryck upp till 1,5 GPa och resultaten visar att tvärbindningsprocesser under högt tryck kan följas i data för κ och ρc_p. Dessutom kan κ för en väl tvärbunden (ebonit-liknande) polymer nära atmosfärstryck och rumstemperatur bli upp till 50% högre än den för det obehandlade materialet, medan ρc_p närmar sig värdena i glastillståndet för det obehandlade materialet. Vidare så sker glastransitionen i ett allt större temperaturintervall och vid högre temperatur med ökande grad av tvärbindning. I nylon-6 orsakar HP&HT behandlingen mikrostrukturella förändringar som ökad kristallinitet och orienterade större kristaller, vilket ökar κ och förbättrar materialets termiska stabilitet.

Mätningar av de termiska egenskaperna för kompositer, visar att κ ökar betydligt, t.ex κ för en komposit med 5 vikt% SWCNTs i PI ökar med 120% jämfört med ren PI. Den kraftiga ökningen i κ förklaras av kolnanorörens höga κ. Inblandning av MWCNTs förbättrar också κ men inte lika mycket som vid inblandning av SWCNTs. Detta beror på lägre aspect ratio (längd/diameter) medan deras lägre κ inte i någon större utsträckning påverkar resultatet. Inblandning av kolnanorör höjer glastransitions-temperaturerna för polymerer. Resultat för SWCNTs i PB visar att glastranstionstemperaturen ökar något mer än vid inblandning av MWCNTs och då speciellt under de mest densifierade förhållandena och för PB med högst molekylvikt, vilket kan bero på att detta ger de mest fördelaktiga förhållandena för PB beläggning (”wrapping”) av kolnanorören.

Mekaniska studier av de HP&HT behandlade polymererna och kompositerna visar att kolnanorör kraftigt ökar draghållfastheten och Youngs modul, t.ex. 5 vikt% SWCNT i PI som behandlats vid 1 GPa och 513 K visar 2 ggr högre draghållfasthet och 2,3 ggr högre Youngs modul än ren PI som behandlats på samma sätt. Resultaten indikerar att behandlingen förbättrar den svaga kraftöverföringen mellan kolnanorören och polymeren, vilket är ett av hindren för att åstadkomma starkare kolnanorörskompositer.

Nyckelord: polymer, kolnanorör, tryck, värmekapacitet, Youngs modul, tvärbindningsdensitet.

Acknowledgements

The years I have spent in Umeå have been among of the best times of my life because during this study period I have met very grateful and kind people. Coming to Ph.D. study in Sweden, a country which is far away from my hometown, Lao PDR, I have had to adapt myself to a new social milieu, academic, and placed myself in this a new physical and social environment for around six years. Here with different background, I have learned culture, livelihoods, and natural environment living of a northern country with cold weather, snow, long night in winter and white night in summer. My feeling is as warm as my home country, particularly the feeling of the warm atmosphere of working and learning at the Department of Physics, Umeå University. Here, I have also learned a lot from my research project, from academic courses. I have done this within my new colleagues at the Department, who have sincerely supported me. Accordingly, I would like to express my thanks here to all those people whom have helped me or had good time together.

First of all, I would like to convey my heartfelt thanks and appreciative warmness to my two supervisors Dr. Ove Andersson and Professor Bertil Sundqvist who have advised and encouraged me to have patience through all difficulties, and who have always motivated me to accomplish my study. I would also like to extend my heartfelt gratefulness to Dr. Ove Andersson who has been my main supervisor during six years of my PhD study. I thank you for your patience in helping me, your constant guidance and advice, your valuable comments and suggestions, and your encouragements during my study period. I am really very happy to have had a dedicated supervisor like you, and I appreciate your openness, trustworthiness, and that you never give up in front of obstacles. You have always helped me to solve all possible problems with your nice and friendly supervision. I would also like to express gratitude to Professor Bertil Sundqvist who has been my co-supervisor, I appreciate your patience advising me, your valuable comments and suggestions, and thanks for organizing everything for my study. I will never forget the two of you for your kind assistance. Without you, I would not be completed my study.

I am grateful to the Swedish Institute, Sida/SAREC, and Umeå University, especially the Physics Department to accept me to study and to provide me a scholarship and academic support during six years study in Sweden. I would like to thank Roger Halling for introducing me to the project, and I would also like to express gratitude to Lena Burström and Katarina Hassler who have been Department coordinators for this project, for your considerations, inspiration and support to my study in Sweden.

In the years as a PhD-student I have besides doing research also spent many hours helping M.Sc student to do experiment in laboratory. I appreciate the confidence that Ove Andersson has shown me when he has visited to researching advice in my country.

I would like to thank to Lena Åström, Tomas Gustafsson and workshop staff, and all people who help me to build the work experiment possibility.

I want to thank Kelley Gundale who has corrected my imperfect English in the first draft of introduction and experimental parts of this thesis. I would like to thank to Aina Tollefsen Sida/SAREC coordinator at UMU, Assoc. Prof. Dr. Khamphong Nammavongmixay Sida/SAREC coordinator at the National University of Laos (NUOL) and Assoc. Prof. Dr. Somchanh Bounphanmy, Vice Dean, and Sida/SAREC coordinator of the Faculty of Science. My thanks also go to the National University of Laos (NUOL), in particular to Prof. Dr. Soukongseng Xayaleuth the president of NUOL and his staff to facilitate documentation process and kind cooperation. I also want to thank all my Lao friends in Umeå, who I share all the difficulties and happiness in a country far away from home.

And last, but not least, I would like to thank all those people whom I am grateful to that I forget to mention their names here.

Finally, I would extremely like to express many thanks to my wife Kenchan, my two sons and daughter to give me an opportunity to study abroad. You are always close to me and thank you for your patience and constant encouragement to my study, even during the time we have lived far away from each other.

Umeå, 2011

Bounphanh Tonpheng

Publications

Included papers

I **Crosslinking, thermal properties and relaxation behaviour of polyisoprene under high-pressure**
Tonpheng B., Andersson O.
European Polymer Journal, **2008**, 44, 2865-2873.

II **Thermal conductivity, heat capacity, and cross-linking of polyisoprene/single-wall carbon nanotube composites under high pressure**
Tonpheng B., Yu J., Andersson O.
Macromolecules, **2009**, 42, 9295-9301.

III **Tensile strength and Young's modulus of polyisoprene/single-wall carbon nanotube composites increased by high pressure cross-linking**
Tonpheng B., Yu J., Andresson B. M., Andersson O.
Macromolecules, **2010**, 43, 7680-7688.

IV **High-pressure-induced microstructural evolution and enhancement of thermal properties of Nylon-6**
Yu J., Tonpheng B., Andersson O.
Macromolecules, **2010**, 43, 10512-10520

V **High pressure crystallization of nylon-6/MWCNTs composites: thermal conductivity and heat capacity, transition studies**
Yu J., Tonpheng B., Gröbner G., Andersson O.
Submitted

VI **Effects of cross-links, pressure and temperature on the thermal properties and glass transition behaviour of polybutadiene**
Tonpheng B., Yu J., Andersson O.
Submitted

VII **Thermal properties and relaxation behaviour of polybutadiene SWCNTs and MWCNTs composites**
Yu J., Tonpheng B., Gröbner G., Andersson O.
In manuscript

In conference proceedings

1. In situ high-pressure vulcanization and thermal properties of polyisoprene
   Tonpheng B., Andersson O.
   High Pressure Research, **2006**, 26(4), 415-419.
   http://dx.doi.org/10.1080/08957950601101852

2. Polyisoprene single-wall carbon nantube composites synthesized under high pressure
   Tonpheng B., Yu J., Andersson O.
   High Pressure Research, **2008**, 24(4), 587-590.
   http://dx.doi.org/10.1080/08957950802444788

3. Thermal conductivity and heat capacity of a nylon-6/multi-wall carbon nanotube composite under pressure
   Yu J., Tonpheng B., Andersson O.
   V International Conference On Times Of Polymers (Top) and Composites, AIP Conference Proceedings, **2010**, 1255, 145-147.
   DOI: 10.1063/1.3455559

Contents

1. INTRODUCTION

This thesis is mainly devoted to the thermal and mechanical properties of polymer-carbon nanotube composites produced by treatment at high pressure and high temperature (HP&HT). A basic understanding of the interaction between the components is important for improving the properties of composites. In this work, HP&HT treatment was used to gain further knowledge about the interaction between nanotubes and polymer chains to improve the physical properties of these new composite materials.

Presently, nanotechnology attracts much attention due to its potential in science and industry, offering new design and improved properties due to their nanometer size. After the discoveries of C_{60} fullerenes in 1985 and carbon nanotubes (CNTs) in 1991, the interest in nanotechnology among the scientific community increased tremendously, this is evidenced by the number of articles published between 1987 and 2007. During these years more than 40 000 papers were published on the topics of fullerence and CNTs [1], and the publication rate increases, more than 14 000 articles about CNTs were published between 2008 and 2011.

In the 1800s, Charles Goodyear invented the vulcanization of natural rubber using sulfur and high temperature, and special agents to interconnect the polymer chains. Vulcanized rubber could be formed to create precise shapes and dimensions. Thereafter, polymers played a very useful role in industry and everyday life as a result of their lightweight and high thermal insulating properties and low production costs. While polymers are easy to process, and their shapes are easy to manipulate, they generally have poor mechanical properties and high sensitivity to temperature change. However, polymer properties can be improved/changed by doping them with various fillers such as fibers, metals, organic and inorganic particles, as well as carbon nano-structured materials, and through physical processing methods, e.g. various pressure and temperature treatments. It is thereby possible to control thermal expansion, obtain improved thermal conductivity and mechanical properties, such as hardness, elasticity, and Young's modulus [2,3,4,5]

Carbon materials are found in a variety of forms such as graphite, diamond, carbon fibers, fullerenes [6], and CNTs [7]. There are two basic types of CNTs: single-wall carbon nanotubes (SWCNTs) and multi-wall carbon nanotubes (MWCNTs), which are produced using three techniques: arc discharge, laser ablation, and chemical vapor decomposition (CVD). Carbon nanotubes have unique mechanical, electrical conductivity, and thermal properties. They are stronger than steel, lighter than aluminum, and more conductive than copper. These properties make nanotubes excellent candidates to substitute or complement conventional nano-fillers used in the fabrication of polymer nanocomposites. Presently, there are only a few nanotube-based commercial products on the market and these are costly. However, if products based on CNTs achieve new and much better properties

than the present ones, these can find use in special applications. Moreover, recent findings indicate that graphene, which is basically an unrolled CNT, has about the same properties as CNTs. Large scale production of graphene will probably be much cheaper than that of CNTs. In any case, the use of these carbon nano-structured materials as advanced fillers, or similar applications, requires intensive studies in order to understand their properties and interaction with other materials. Only when a more profound understanding has been achieved, it will be possible to fully utilize their unique properties in applications such as composites.

Considering the high strength of CNTs, there is a large potential for significant reinforcement of polymer matrixes by inclusion of CNTs, which has recently been reviewed [8,9]. However, the transfer of load to the high strength CNTs conveys a significant problem because of the normally weak interfacial interaction between the matrix and the CNTs. To achieve substantial reinforcement it is, therefore, crucial to find ways to improve the interfacial interaction, otherwise, the CNTs will be pulled out of the matrix. Recent interesting attempts have employed functionalized CNTs, which can both improve the dispersion of the CNTs, and provide a site for obtaining strong bond and/or entanglement between the CNTs and the matrix [3].

The main objective of this study was to explore the change of mechanical and thermal properties of CNT-polymer composites subjected to extreme pressures, and to use the results to better understand the interaction between the CNTs and polymer chains. In particular, we have studied issues such as interfacial thermal resistance and interfacial stress transfer, and observed nano-induced phenomena, e.g. crazing, heat capacity suppression and density enhancement. This was accomplished by high-pressure, in-situ, studies of the thermal conductivity (κ) and heat capacity per unit volume (ρc_p), on both pure polymers and their various CNT composites. Similarly, mechanical studies of the Young's modulus (E) and tensile strength (σ) were done on both pure polymers and their CNT composites after these had been subjected to identical high pressure high temperature treatments, which for some polymers induce cross-links. The main advantage of high pressure studies is that pressurization can decrease the interfacial thermal resistance between CNTs themselves, and between CNTs and the polymer matrix. The decrease of the inter-CNTs distance can also induce percolation, which is a better method than to increase the amount of CNTs, which increases the tendency of CNT bundling. Moreover, high pressure treatment can augment nano-induced effects since the interaction between the CNTs and the polymer chains increases.

This thesis is based on 7 papers. I have also presented research results at the 44th and 46th European High Pressure Research Group (EHPRG 44 and EHPRG 46, respectively) conferences.

2. BASIC CONSIDERATIONS

2.1 Carbon Nanotubes Materials

2.1.1 Discovery and structure

In 1985, Richard E. Smalley, Robert F. Curl and Harold W. Kroto with co-workers [6] discovered the C_{60} molecule, which is also called Buckminsterfullerene, in a laser ablation experiment which was originally designed to study the mechanism by which long-chain molecules are formed in interstellar space. The C_{60} structure is made of 12 pentagons and 20 hexagons arranged to form a truncated icosahedron (see **figure 1**). Thereafter, in 1991, Sumio Iijima discovered multi-layer graphite sheet cylinders on the electrode's deposits by changing the arc power supply to direct current from alternating current during a study of arc-evaporation synthesis of fullerenes [7]. These were named multi-walled carbon nanotubes (MWCNT) (see **figure 2**). Shortly thereafter, in 1993, single-walled carbon nanotubes (SWCNTs) were discovered by Iijima and coworkers [10] at NEC, and Bethune and coworkers [11] at IBM. The discovery of these new structures ignited a lot of scientific interest and intense studies on the synthesis [12,13], structure [13,14], properties [12,14,15,16], and applications [13,15,16] of these materials have been carried out. A more detailed description of the structures is given below and in Refs [14,17].

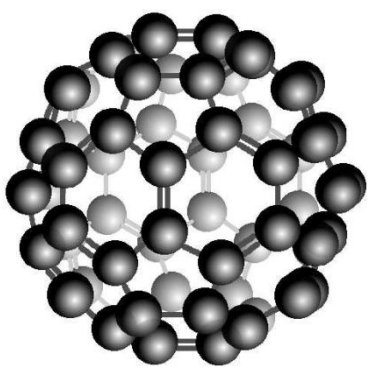

Figure 1. The icosahedral C_{60} molecule[1].

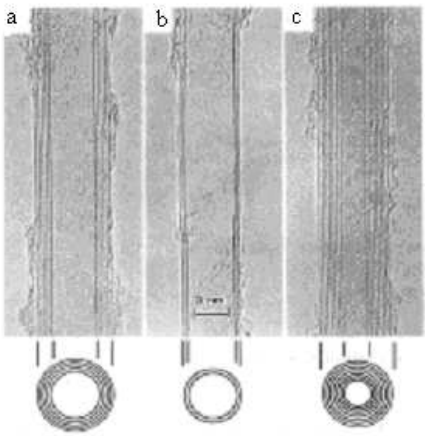

Figure 2. Transmission electron microscopy (TEM) images of the first observed MWCNTs [7]. (a) tube consisting of five rolled-up graphene sheets, diameter 6.7 nm, (b) two sheets, diameter 5.5 nm, and (c) seven sheets, diameter 6.5 nm.

Although Iijima is credited with their discovery, CNTs were probably already observed in 1950s, when Bacon [18] was studying the melting of graphite under high temperature and pressure. Bacon presented the observation of "graphite whiskers" based on an electron microcopy investigation of his material in 1960 and he proposed a scroll-structure [18]. In 1970s Endo showed nanotubes via high resolution transmission electron microscopy (HRTEM) when he explored the production of carbon fibers. Endo observed carbon fibers with a hollow core and a catalytic particle at the end [19,20,21], and discovered that this particle was iron oxide from sand paper. It is now known that iron oxide is as a catalyst for the production of carbon nanotubes.

2.1.2 Structure of carbon nanotube

Carbon nanotubes are considered to be rolled-up carbon graphene sheets that form concentrical cylinders. Nanotube diameters are typically in the range of several nanometers and their lengths can be a few orders of magnitude longer. The properties of carbon nanotubes are strongly dependent on their structures, which is described in terms chirality, that is the orientation of the chiral vetor $\mathbf{C}_h$ (see **figure 3**a) and the chiral angle, θ. The chiral vector defines the way in which a nanotube is rolled-up, and it is described by [22]:

$$\mathbf{C}_h = n\mathbf{a}_1 + m\mathbf{a}_2 \qquad (1)$$

where $\mathbf{a_1}$ and $\mathbf{a_2}$ are unit vectors of the hexagonal lattice, and the indices n and m are integers ($0 \le |m| \le n$). It shows the number of steps along the zigzag carbon bonds of the hexagonal lattice. The chiral angle, θ, is defined as the angle between $\mathbf{C}_h$ and $\mathbf{a_1}$, and the diameter, d_t of a nanotube is calculated from n and m as follow[22],

$$\cos\theta = \frac{2n+m}{2\sqrt{n^2+m^2+nm}},$$

or

$$\sin\theta = \frac{\sqrt{3}m}{2\sqrt{n^2+m^2+nm}}. \qquad (2)$$

$$d_t = \frac{|\mathbf{C}_h|}{\pi} = \frac{a_{C-C}\sqrt{3}}{\pi}\sqrt{n^2+m^2+nm}, \qquad (3)$$

where a_{C-C} is the nearest neighbour distance in graphite (1.42 Å).

By rolling up a graphene sheet in different ways (see **figure 3**b) produces different types of nanotubes referred to as: zizag (from (○) to (□) see **figure 3**b), armchair (from (○) to (△)) and chiral (all intermediate cases). Both zigzag and armchair tubes are considered to have no chirality, whereas all other (n,m) tubes are referred to as chiral. As shown in **figure 4**, the nanotubes may be capped at the end by hemispheres of the buckyball structure.

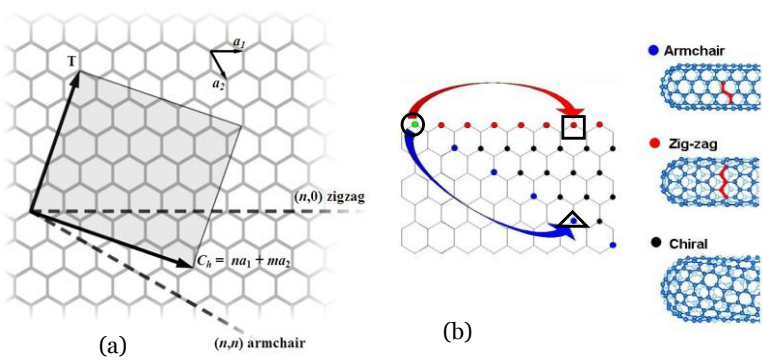

Figure 3. (a) Chiral vector on a graphene sheet [22,23], (b) the following types of nanotubes are possible: armchair, zizag, or chiral by rolling a graphene sheet in different direction [24].

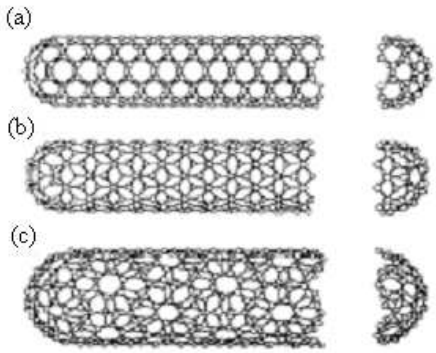

Figure 4. The 3D graphite crystal of single layer of carbon atom, (a) the armchair tubule (5,5), (b) the zigzag tubule (9,0) and (c) the chiral tubule (10,5) [22].

The unit cell of the carbon nanotube is the rectangle bounded by the vector $\mathbf{C}_h$ and **T** shown in **figure 3**a, where **T** is the 1D translation vector of carbon nanotube, which extends from the origin to the first lattice in the honeycomb lattice and it is normal to $\mathbf{C}_h$. The vector **T** in term of the integers (t_1, t_2) is given by:

$$\mathbf{T}= t_1\mathbf{a}_1+t_2\mathbf{a}_2 \ . \qquad (4)$$

The length of **T** is $T=\sqrt{3}|\mathbf{C}_h|/d_R$, where d_R is the highest common divisor of ($2n+m$, $2m+n$) that is $d_R=d$ (if $n-m$ not a multiple of $3d$) or $d_R=3d$ (if $n-m$ a multiple of $3d$), and d is defined as the largest common divisor of (n, m).

There are two main kinds of CNTs: single wall carbon nanotubes (SWCNTs) and multi wall carbon nanotube (MWCNTs). SWCNTs are hollow cylinders, which consist of one rolled-up graphene sheet, with diameters in the range 0.7 to 10 nm, but normally less than 2 nm, and length of order of micrometer. Consequently, these nanotubes have a large aspect ratio, i.e. length/diameter ($\approx 10^4$-10^5) [25]. A MWCNT consists of an array of cylinders formed concentrically around a central hollow core with interlayer separations of ~0.34 nm [26,27], which is the same as for the graphene layer spacing of graphite, with diameters in the range from several nanometers up to about 200 nm [13,15].

2.1.3 Synthesis

One of the most important issues for development of nanotube technology is the progress in production of high purity low-cost nanotubes. CNTs can be synthesized by various methods [12,14,25]. Here, the most common methods are described and these include: arc discharge, laser ablation, and thermal synthesis.

• **Arc discharge**: this method was the first recognized method for producing both SWCNTs and MWCNTs. It uses a low-voltage (~12 to 25 V) but high-current (50 to 120 A). The arc electrodes typically have a cross-section diameter in the range 5 to 20 mm, and the gap between the electrodes, which consist of graphite, is ~1 mm. The production process requires Argon or Helium gas at a pressure of 100 to 1000 Torr (see **figure 5**) [13]. Several catalysts have been used but the best yield of nanotubes has been obtained for Ni, Co and bimetallic system such as Ni-Y, Co-Ni, Co-Pt. The use of a Ni-Y catalysts (in a 4 to 1 ratio) in this method has provided very high yield (>75%) of SWCNTs [28]

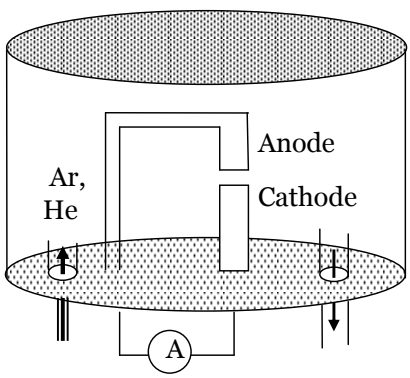

Figure 5. Schematic drawing of an arc discharge chamber [13]

• **Laser ablation**: this method was established by Smalley's group at Rice University in 1996 [29]. In this case, a graphite target (e.g. Co-Ni or Ni-Y), which is placed in a quartz tube at 1200°C is vaporized by laser irradiation under a flow of inert gas at 500 Torr (Ar or He gas) as shown in **figure 6**.

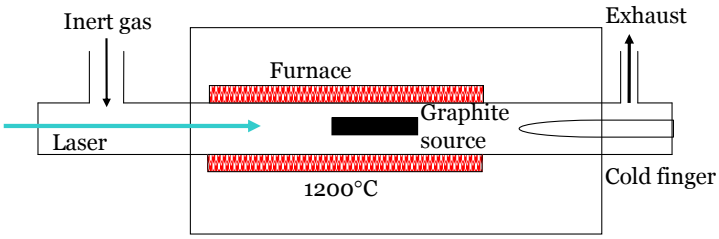

Figure 6. Schematic of a laser ablation furnace[13].

• **Thermal synthesis**: this method can be divided into a few subgroups: CVD, HiPco, and flame synthesis are all considered as thermal methods for CNTs synthesis.

- Chemical vapor decomposition (CVD): Endo *et al.* [30] were the first to report production of MWCNTs by this method, and then Smalley's group successfully adapted CO-based CVD to produce SWCNTs [31]. In CVD, a gaseous carbon source is decomposed catalytically, and the nanotubes are deposited on a substrate or grown from a substrate (see **figure 7**). The SWCNTs can be produced from 0.4 to 5 nm in diameter [13], and these are almost completely free of amorphous carbon. MWCNTs are mainly obtained by this method and it yields long nanotubes with diameters in the range 10-200 nm [32,33,34].

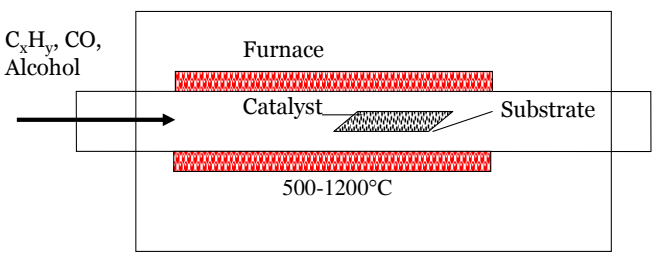

Figure 7. Schematic figure of a CVD furnace[13].

- High pressure conversion of carbon monoxide (HiPco): this method is an improved CVD synthesis, which is based on gas-phase growth at high temperature and high pressure conditions where carbon monoxide provides the carbon source (**Figure 8**)[13,35,36]. This process gives SWCNTs with diameters in between 0.7 and 1.1 nm[13], with a production rate up to 15 mg/h [37].

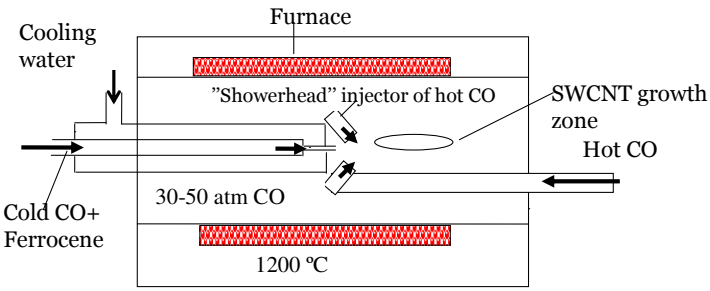

Figure 8. Schematic figure of a HiPco furnace [13]

The extracted samples in carbon nanotube productions inevitably include amorphous carbon, carbon nanoparticles, and catalyst residues, which are desirable to remove. However, purification may not be trivial, as any treatment designed to remove metal catalyst particles and amorphous carbon can often result in functionalization of the tubes and/or the introduction of defects into the structure of the nanotubes. The most commonly used purification methods include oxidation [38], filtration [39,40] or chromatography [41,42]. In our work, we purified MWCNTs by oxidation in air before making the composites (Nylon-6 see **paper V**).

2.1.4 Properties of CNTs

The general properties of nanotubes have been discussed in a number of publications as mentioned above. Here, only brief accounts of their most important properties are given and these include the mechanical, thermal, electrical, and optical properties. More detailed and comprehensive descriptions are given in Refs. [12,13,17,25,43,44,45].

2.1.4.1 Mechanical properties

The elastic properties of CNTs are determined by the three kinds of forces that arise in the CNTs: two types of strong intralayer carbon-carbon bonds and one weak interlayer interaction (only MWCNTs) [25]. The intralayer forces consist of strong σ bonding and π-bonding forces between the carbon atoms, which give nanotubes very high Young's modulus and tensile strength. These properties were studied theoretically already in 1993 by Overney *et al.* [46], who used computer calculations to investigate rigidity and low-frequency vibrational properties of CNTs. They found a Young's modulus of ~1.5 TPa by studying the bending of a carbon nanotube with 200 carbon atoms, which was clamped on one side and free on the other. A more recent study reports a Young's modulus of 1.0 TPa [47]. These values are

about the same or only slightly larger than 1.1 TPa found in the basal plane, or the graphene layers, of graphite [48], 0.5 TPa for suspended graphene sheets [49] and ~1.1 TPa for diamond [50]. Subsequent experimental investigations have yielded results that are in fair agreement with the predictions. Yu *et al.* [51] measured force-strain data for SWCNT ropes and deduced that a model in which the load was carried only by the SWCNTs on the perimeter of the rope best fitted the experimental results. Based on this model, they reported Young's moduli for SWCNTs in the range 0.32-1.47 TPa, with a mean of 1.00 TPa. Moreover, the same model yielded tensile strengths in the range 13-52 GPa. Other experimental and theoretical investigations also show extraordinary mechanical properties of individual MWCNTs with Young's modulus being over 1 TPa and tensile strengths in the range 10-100 GPa [52,53]. It is therefore obvious why CNTs have been frequently tried as reinforcement filler in composite materials, and the potential of obtaining strong structures have been demonstrated by the production of very strong ribbons [54], yarns [55,56], and fibers [57]. For more details see e.g. [12,25,58].

2.1.4.2 Thermal properties

Carbon nanotubes are of great interest not only for their high strength and modulus, but also for their thermal properties and, in particular, their high thermal conductivity. In the classical Debye model [59], the thermal conductivity depends on three parameters: the phonon mean free path (or relaxation time), the phonon velocity and the phonon heat capacity. Due to their nanoscaled size, quantum effects are expected, and the specific heat and thermal conductivity show direct evidence of 1 D quantization of the phonon band-structure [60]. Some nanotubes have high electrical conductivity and in general both electrons and phonons can contribute to the thermal conductivity. However, in graphite, the phonons dominate the heat capacity down to 20 K and for CNTs even down to near 0 K [12]. It follows that the electronic part of the thermal conductivity for CNTs is neglible in the temperature range studied here.

Hone *et al.* [60] calculated the phonon specific heat for an isolated (10,10) SWCNTs, a graphene sheet, and graphite. They found that at low temperatures (below 50 K), the specific heat of the SWCNT is significantly lower than that for a graphene sheet, which was attributed to the stiffening of the acoustic modes due to the cylindrical shape of SWCNTs. In the low temperature range, below about 5 K, the calculated specific heat of a SWCNT is linear in temperature, which is a behavior characteristic of a 1-D system. Above 5 K, the measured specific heat of SWCNTs bundles agrees well with the predicted curve based on the calculation for individual (10,10) SWCNTs. At high temperature above 100 K [60], specific heat results of SWCNTs also agree well with the predicted, graphene, graphite (phonon) and SWCNTs bundles curves. Yi *et al.* [61] used a self-heating technique to measure the specific heat of CVD-produced MWCNTs and they found a linearly increasing specific heat from 10 K to 300 K. Below 100 K, the results were in

better agreement with graphene than graphite, which was attributed to weak interlayer coupling in their MWCNTs.

The thermal conductivity of CNTs depends on the specific heat and the diagonal term of the thermal conductivity tensor, which is a sum over all phonon states, can be written as [12]

$$\kappa = \frac{1}{3}\rho C v^2 \tau_s , \qquad (5)$$

where C, v, and τ are the heat specific heat per unit volume, group velocity, and relaxation time of a given phonon state, respectively. The group (phonon) velocity is more or less constant through a wide temperature range [62]. Thus the changes in κ with temperature should be governed by the changes in heat capacity and relaxation time.

In case of SWCNT ropes, phonons propagate both along individual tubes and between parallel tubes in the hexagonal lattice, and disperse in both the longitudinal (on-tube) and transverse (inter-tube) directions. Turning to the MWCNTs, their phonon dispersion relations have not yet been addressed theoretically as has been done for the SWCNTs. But due to the lack of "strict registry" between the layers in a MWCNT, it has been suggested that the interlayer coupling would be much weaker than in graphite [12], which should limit the heat flow between the layers.

The thermal conductivity (κ) of SWCNTs has been investigated both theoretically [63] and experimentally [64,65]. A molecular dynamics simulation of an isolated (10,10) SWCNT indicates that κ is 6000 W m^{-1} K^{-1} at room temperature and that it increases with decreasing temperature down to 100 K, where it peaks at 37 000 W m^{-1} K^{-1} [66]. However, bulk samples have much lower κ due to the weak inter-tube coupling, which gives a large thermal resistance between individual CNTs. Hone *et al.* [64] measured κ of laser-vaporization produced bulk samples of SWCNTs with a typical diameter of 1.4 nm and reported that $\kappa(T)$ increased with increasing temperature from 8 K to 300 K, which thus is different from that of the isolated SWCNT as well as normal crystals with sizes of order of micrometer or larger. Experimental results for the latter show a maximum in κ as a function of temperature, typically below 100 K, in correspondence with the result for an isolated SWCNT, and then κ decreases when the dominant phonon scattering mechanism changes from boundary to Umklapp scattering. Thus, even if Hone *et al.* [12], suggested that a gradual decrease in the slope of κ for SWCNTs above 250 K indicated the onset of Umklapp scattering, the heat transport in bulk SWCNT samples seems far from that of normal crystal. A likely reason for this difference is the weak inter-tube coupling.

The κ of CVD-grown MWCNTs, measured from 4 K to 300 K [61], varies as T^2 below 120 K, which is similar to the $\kappa \sim T^{2.3}$ behavior of graphite. Moreover, like bulk SWCNT samples, $\kappa(T)$ of the bulk MWCNT sample do not display a maximum. The magnitude for κ of individual MWCNTs was measured by Kim *et al.* [67] who found κ ~3000 W m^{-1} K^{-1} at room temperature.

2.1.4.3 Electrical properties

CNTs possess unique electrical properties and the conducting properties are closely related to the molecular structure. More specifically, a CNT's band structure depends on its chirality, and it is either that characteristic of a metal or a semi-conductor [53]. It is therefore possible to identify metallic or semiconducting tubes through the chirality, where the former are those with $n = m$, i.e. armchair structure (see section 2.1.2), or with $n\text{-}m = 3i$ (where i is a integer). In all other cases, the CNTs have semiconducting properties [13,68]. For example, a (7,1) tube would be metallic, a (8,0) tube semiconducting, and a (5,5) armchair tube metallic.

An electrical current of up to 25 μA can be passed through a metallic SWCNT, which corresponds to a huge current density of 10^9 A cm^{-2}. Moreover, individual purified MWCNTs have a current density in excess of 10^7 A cm^{-2}, with a high electrical conductivity, ~2×10^3 S cm^{-1}, along the long axis [69]. In addition, the CNT length and temperature dependence of SWCNTs electrical properties have also been studied [70,71]. For semiconducting CNTs it is important to know that these have a band gap that scales inversely with tube diameter [69].

2.1.4.4 Optical properties

This section gives a brief description of Raman spectroscopy results for CNTs. Raman scattering has proven to be a very important tool for characterizing SWCNTs [72]. This is mainly due to the one-dimensional confinement of its electronic and phonon states, which gives van Hove singularities in the CNT density of states. These cause resonance in Raman scattering, which provide detailed information about CNTs. Raman results for CNTs reveal peaks that depends on the structure of the CNTs, e.g. chirality and CNT diameter, because each CNT has a very distinct set of allowed transitions. For example, a Raman spectrum of a SWCNT shows only three main peaks as shown in **figure 9**. One at low Raman shifts (≈186 cm^{-1}), which is due to the radial breathing modes (RBM) and the shift depends on the CNT diameter [68], i.e. it can be used to estimate the diameter [73,74]. Two other peaks are called D- and G-band. The D-band, which is attributed to defects in the sample, is at about 1300 cm^{-1}, and the G-band, which is characteristic of graphite, occurs at around 1600 cm^{-1} [12,13,68]. More specifically, the Raman spectrum of arc-discharge SWCNTs reveals a D-band at 1308 cm^{-1}, G-band at 1532 and 1569 cm^{-1} and a G´-band at 2610 cm^{-1} [75]. Kwok *et al.* [76] reported the Raman spectrum of CVD

grown MWCNTs and for those the D-band and G-band occur at about 1353 $cm^{-1}$and 1583 cm^{-1}, respectively.

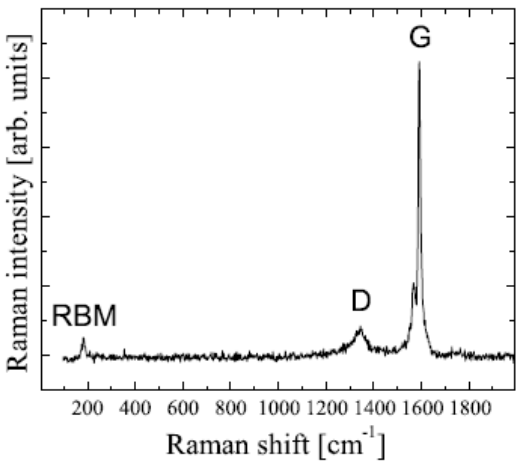

Figure 9. An example of Raman spectrum of SWCNTs [1].

2.1.5 Carbon nanotubes applications

Since Iijima discovered CNTs in 1991 [7], these have been the subject of intense interest because of their potential in applications. Their properties and size, with high aspect ratio, have been arguments for use as advanced filler in composite materials based on e.g. polymers, ceramics, and metals to enhance or add some property. CNTs are also being considered for use in energy production and storage. In addition to their large surface area, their high electrical and thermal conductivity, high strength and toughness makes these interesting for use in fuel cells, batteries and capacitors. Fast electron transfer kinetics on CNTs have been demonstrated [77], which suggests that these can be used as electrodes for various electrochemical applications (e.g. fuel cells), and CNTs have been tested as base for catalyst particles for oxygen reduction reactions [78]. Moreover, CNTs can be a good candidate for improving batteries, which require high energy capacity, fast charging time and long cycle life [79,80].

It has been demonstrated that supercapacitors with carbon nanotubes electrodes show a specific capacitance (capacitance per unit mass) of 380 F/g [81] (commercial supercapacitors have capacitances up to 5000 F but then these have a mass of 900 g) [82]. In another study, a SWCNT based supercapacitor obtained a specific capacitance of about 180 F/g, power density of 20 kW/kg and energy density of 7 Wh/kg in a KOH electrolyte [83]. In a more recent study, MWCNTs were used for the same application reaching a specific capacitance and energy density of 270 F/g and 317

Wh/kg, respectively [84]. Lithium batteries based on functionalized MWCNTs electrodes can store lithium up to a reversible gravimetric capacity of 200 mAh/$g_{electrode}$ while also delivering 100 kW/$kg_{electrode}$ of power [80]. Nano-sized electronic devices, such as nanotube field effect transistors (NT-FETs) have also been achieved. Moreover, because of their small size, CNTs can improve the resolution in scanning tunneling and atomic force microscopes, as well as other scanning probe instruments. Many other potential uses have also been suggested, and some of these are described in the Refs. [12,13,14,85,86].

2.2 Polymers

The word polymer originates from the Greek words poly and mer. The former means many and the latter means parts, i.e. polymer means something consisting of many parts, or repeat units. The repeat units of the polymers studied in this work are: [$CH_2CH=C(CH_3)CH_2$] (polyisoprene, PI), [CO-(CH2)5-NH] (Nylon-6), and [$CH_2CH=CHCH_2$] (polybutadiene, PB). The polymer consists of a large number of these, which are connected by covalent Carbon-Carbon bonds. To improve or change the mechanical properties of polymers, these are often cross-linked, which means that the polymer chains are bonded to each other forming a network polymer. The most well-known example is cross-linked polyisoprene, which makes an elastic polymer that is commonly referred to as “rubber”.

2.2.1 Polyisoprene

In general, rubber materials contain fillers e.g. carbon, silica and clay or whiting. A rubber material is normally produced using a vulcanization system whose primary purpose is to crosslink the polymer. Natural rubber (NR) is one important material, which have been widely used in industry and daily life. Natural rubber is obtained from the rubber tree, *Hevea Brasiliensis*, and it consists of many different components: about 94% *cis*-1,4-polyisoprene, with 2.2% of proteins and 3.4% of lipids as known contaminants[87]. The roll of fillers in rubber materials is to tailor the properties of the final product. In addition to the polymer and filler, vulcanized rubber also contains cross-linking agents, accelerators, activators and retarders of the cross-linking reaction, i.e. a vulcanization system. The composition of the vulcanization system, polymer and filler can be varied to modify the properties of the rubber material.

PI, i.e. the main component of natural rubber, has a highly regular structure consisting primarily of linear sequences of *cis*-1,4- and *trans*-1,4-units, as shown in **figure 10**, and vinyl units which result from the polymerization of the isoprene monomer. The monomer, isoprene, is highly reactive, capable of polymerizing when heated or by use of catalysts. PI is

amorphous under normal condition, but may crystallize on stretching. Almost all of the poly(isoprene) production is devoted to *cis*-1,4-poly(isoprene), i.e. the synthetic version of the major polymer in natural rubber.

The uses of PI are numerous and widespread, *e.g.* PI is used for making thermo-plastic materials such as telephone handsets, refrigerator liners, safety helmets and radio components, roofing, flooring, paints and adhesives.

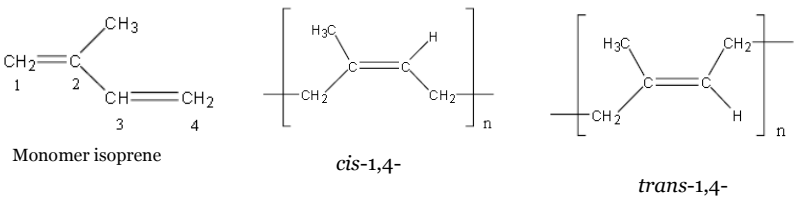

Figure 10. Chemical structure of PI [88].

A typical Fourier transform infrared (FTIR) spectrum of our PI sample is shown in **figure 11**. The sample consists of mainly *cis*-1,4 PI, but should also contain small amount of the *trans* configuration. Raman and FTIR spectra can be used to quantify *cis*-1,4- and t*ran*-1,4- configurations using the observed bands for each configurational structure type, as shown in [89, 90]. Although there are differences in the spectra of the *cis* and *trans* isomers, which can be used to study mixed samples [90], the differences are small and the minute amount of *trans* isomer in the sample could not be detected in the spectra. In **figure 11,** peaks for the CH_2 stretch appear at 2925 cm^{-1} and 2854 cm^{-1}, those for the CH_2 deformation at 1447 and 1375 cm^{-1} and that for the stretching mode of the carbon-carbon double band at 1664 cm^{-1}.

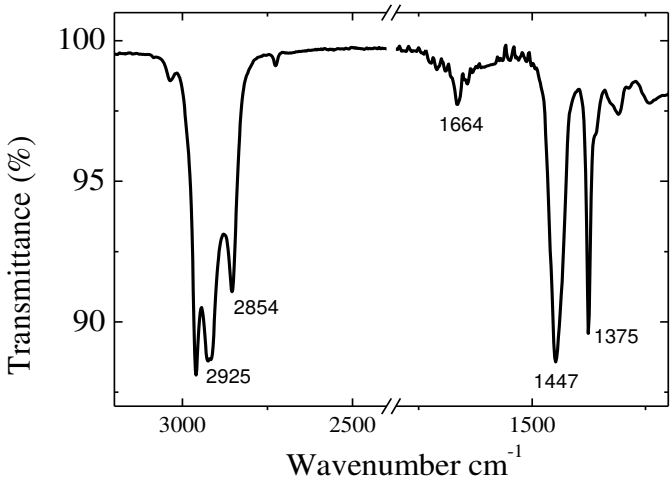

Figure 11. A FTIR spectrum of polyisoprene used in this study.

2.2.2 Polybutadiene

Butadiene rubber typically consists of a mixture of *cis*-1,4-PB, *trans*-1,4-PB, and 1,2-PB. The molecular weight (M_n= number average) is commonly over 100 000 g/mole and a chain contains over 2 000 butadiene repeat units. The physical properties of PB depend to a large extent on the distribution of the monomer unit among the three configurations i.e. *cis*-1,4, *trans*-1,4 and 1,2 (*vinyl*).

2.2.3 Nylon-6

Nylon-6 is a semicrystalline polymer, which in our case had a stated number-average relative molecular mass of 10 000 g/mol. The crystalline part has a thermodynamically stable monoclinic α structure, which gives nylon-6 high strength, good temperature and chemical resistance [91]. Nylon-6 is therefore an important engineering thermoplastics and a suitable matrix for composites materials. Nylon-6 is not a condensation polymer, but instead it is formed by ring-opening polymerization, i.e. a form of chain-growth polymerization (polyaddition) in which the terminal end of a polymer acts as reactive center.

2.2.4 Polymer network and cross-linking

Cross-linked polymers, or network polymers, have generally higher Young's modulus and tensile strength than the corresponding polymer without cross-links. In fact, the polymer could even be in a liquid state without cross-links, which is the case for the polyisoprene sample studied here. At low or moderately high cross-link densities, the polymer could be in an elastic state, and progress towards a glass-like or ebonite-like state with increasing cross-link density. Cross-links, or chemical bonds between the polymer chains, are formed by chemical reactions that are normally initiated by heat and/or by mixing with various chemicals, but can also be induced by radiation and pressure, and the latter was the method used in this study. The properties of the cross-linked state depend strongly of the cross-link density, i.e. the number of cross-links per unit volume, which is commonly expressed in mol cm^{-3}. The cross-link density is inversely related to the average molecular weight of the chains between the cross-links, which is an alternative way to express the network properties.

The degree of cross-linking of rubber-like samples may be estimated by several different methods, and in this work we have used the swelling method. It is described in detail in the experimental method section and also with fewer details in **paper I**. Another method is based on tensile stress-strain measurements, but in the beginning of this project it was not possible due to the lack of a tensile tester. Although it was not employed, it is described here briefly for completeness. The measurements are done using strips cut from cross-linked samples. Values of the molecular weight M_C between cross-links are calculated from a relation given by the simple kinetic theory of rubber elasticity [92]

$$M_C = 3\rho RT / E , \qquad (6)$$

where R, T, ρ and E are the gas constant, test temperature, polymer density, and tensile (Young's) modulus, respectively. The Young's modulus is obtained from the initial slope of the stress vs. strain curves.

The molecular weights of polyisoprene typically vary from about 1 000 to 60 000 g/mol, and the sample used in this work had a molecular weight of 38 000 g/mol. The molecular weight M_C between cross-links for cross-linked natural rubber samples is normally in the range 1 000 to about 17 000 g/mol [92]. Thus, a typical natural rubber has a cross-link density (=$1/M_C$) in the range 10^{-3} to 10^{-5} mol/cm^3. These can be both chemical (bonds) and physical cross-links (entanglements), which are formed due to a reaction and as a consequence of long polymer chains. The entanglement limit for polyisoprene, i.e. the limit below which physical cross-links do not form, is estimated to about 10^4 g/mol [93]. Chemical cross-linking arises when a rubber material is vulcanized, or in any other way treated so that new bonds are created between individual polymer chains.

2.2.5 Polymer vulcanization

The discovery that raw rubber polymer can be converted into an elastic material by heating in contact with various chemicals is attributed to Goodyear who patented his finding in America in 1944. This process was called vulcanization and it initially involved the utilization of sulfur. Subsequently, it was further developed using various chemicals that, for example, accelerates the process to shorten the time and/or to decrease the temperature needed for completion. Nowadays vulcanization refers to the process by which a polymer is cross-linked using cross-linking agents, activators, accelerators and retarders of cross-linking, e.g. peroxides (agent) and zinc oxide (activator), or sulfur and white lead [94], as in Goodyear's original discovery of the vulcanization process. Vulcanization is thus a chemical process whereby individual polymer chains are linked to other polymer chains by atomic bridges composed of sulfur atoms or by carbon to carbon bonds. The end result is that the springy rubber molecules become locked together (cross-linked) to a greater or lesser extent. The bulk of the polymer becomes harder and less sticky, which makes it more durable and resistant to chemical attack and thermal degradation.

The vulcanization technique has been developed during the years to fit new materials and to meet the demands of modern production of rubber materials, but still it is remarkably similar to the original process. Many products are made with vulcanized rubber ranging from tires, shoes, hoses, seals and vulcanite (ebonite) to bowling balls and clarinet mouth pieces. Despite the importance of vulcanization, relatively few studies have concerned the possibility of a similar process by treatment under high pressure which would not require chemical agents and could lead to modified properties because of the densified conditions during the process. But perhaps even more importantly, it can be used to study cross-linking in polymers and its influence on polymer properties as well as the interaction between a polymer matrix and nano-fillers, in particular, that between CNTs and polymer matrixes.

2.3 Carbon Nanotube-Polymer composites

A polymer nanocomposite consists of a polymer matrix with a nano-sized filler. Many different fillers have been tested and is also used commercially to improve or modify the properties of polymers and some of these have nano-size. In this context, CNTs is one of the most interesting filler for future applications. Because of their extraordinary properties and large aspect ratio, minute amount of CNTs can have an unusually large influence on the properties of a composite. But the changes in the composite properties have so far not reached the expected sizes and to achieve better results may require better understanding of their interaction with (polymer) matrixes.

These studies are, however, complex and it can take many years until the best conditions are established and this is due to several reasons. CNTs's own properties depend on many factors: single wall or multi wall, chirality, CNT diameter, length, (aspect ratio), impurities and defects, which depends on the production process used to produce the CNT, purification process, etc. The production of composite increases the difficulty since it requires homogeneous dispersion of the CNTs in a polymer matrix, and CNTs tend to agglomerate in bundles. The CNT orientation in the polymer matrix will also affect the properties. If simple procedures to produce well-dispersed and homogeneous CNT-polymer composites are developed and the conditions for e.g. full structural reinforcements by the CNTs can be fulfilled, it has been predicted that such composites can become extremely strong. Because of the high cost of CNTs this could presently be useful in highly specialized applications as, for example, composites for ultra-light-weight thin-walled structures for use in space (e.g. aerospace structural panels and high stiffness-to-weight space mirror substrates [95]). Numerous other applications have been suggested and several concern nonlinear optics [96] such as advanced protection of human eyes, optical elements and optical switching.

2.3.1 Production of CNT-polymer composites and methods for achieving good dispersion and improved interfacial interaction

The superior properties of CNTs offer exciting opportunities for composites. Although CNTs have a very high specific surface area $>10^3$ m^2/g for SWCNTs and 50 m^2/g for MWCNTs [97], which makes the interface between polymer and filler very large, it still seems insufficient to obtain the required load transfer between the matrix and CNTs to reach maximum reinforcement. The observed increases of thermal conductivity in polymer-CNT composite are also rather moderate, which is likely due to a large thermal resistance between the CNTs and the polymer. Another reason for moderate changes in the properties of the composites is that CNTs easily agglomerate, or bundle together in a highly entangled network structure, which is difficult to disperse and the composites therefore become inhomogeneous.

Several techniques have been tested to improve the interaction to prevent slippage between polymer and CNTs, and various methods are used to optimize the dispersion of CNTs. Here, the most common techniques are described and these includes: solution blending, melt blending, and in situ polymerization, which are widely applied to produce nanotubes-polymer composites:

- ***Solution blending***: This is the most common method for fabricating small samples of CNTs-polymer composites, and it is effective in

producing relatively well dispersed CNTs, when high-power ultrasonication is used for a long period of time. Solution blending involves three major steps: (i) dispersing CNTs in a suitable solvent, (ii) mixing CNTs with the polymer (at room temperature or elevated temperature), and (iii) evaporating the solvent. To avoid that the CNTs agglomerate during the slow solvent evaporation it is important to continue the sonication until the viscosity increased enough to limit the CNT diffusion. The time for the solvent evaporation can be reduced by pumping and/or heating.

- ***Melt blending***: In this case, the polymer is heated to temperatures near the melting point and the CNTs are mixed in the polymer, e.g. by a screw extruder. This technique is a common alternative, and it is probably the most easy method to scale up for industrial production. However, the dispersion of the CNTs is often inferior that achieved in solution blending.

- ***In situ polymerization***: This method is suitable for insoluble and thermally unstable polymers. The initial step is to disperse the CNTs in the monomer, which is followed by polymerization. This technique is a very convenient processing technique that allows the preparation of composites with high CNT loading and it can yield very good dispersion with almost any polymer type. For example epoxy nanocomposites have been successfully processed using in situ polymerization methods [98,99,100].

- ***Functionalization of CNTs***: This technique is, for example, used to promote dispersion in a matrix and improve the interfacial interaction with the matrix. Covalent functionalization, amino-functionalized CNTs and the surface chemistry of carbon have been envisaged as very important factors for nanotubes processing and applications. In a typical functionalization process, CNTs are treated using high concentration acids to introduce carboxylic group (-COOH), followed by further functionization using amine molecules [101,102,103,104].

Although it is possible to obtain relative good dispersion of the CNTs, simply mixing the CNTs in a polymer may not be sufficient for optimizing mechanical and other properties of the composites. Specialized techniques may be employed for e.g. controlling the CNT orientation and for increasing the load transfer. In this context, functionalized nanotubes have been tested, which can both improve the debundeling and provide sites to form covalent bonds between the matrix and the CNTs [105,106] , as shown schematically in **figure 12**. In this thesis work, it has been tested to improve the interfacial contact by cross-linking the matrix under densified conditions.

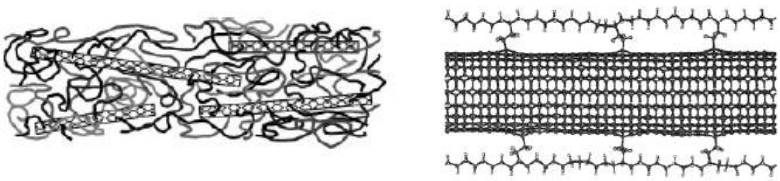

Figure 12. Illustration of the cross-linked system, *left* [105], and a schematic figure of CNTs bonded with a matrix, *right* [106].

2.3.2 Properties of carbon nanotube-polymer composites

2.3.2.1 Mechanical properties

In this section, the parameters determining the strength of CNT composites are discussed. The understanding how these are affected by various production methods and changes in matrix and CNTs are vital for fabrication of composites that take full advantage of the CNT properties to make light polymer-based composites, which are mechanically stronger and tougher than the pure polymer [107,108,109,110]. The strength of CNTs polymer composites depends mainly on two variables:

- Degree of load transfer between the matrix and the nanotubes. If the interfacial adhesion between the phases is weak, the nanotubes behave as holes or nanostructured flaws, inducing local stress concentrations [111,112], and the CNTs can be pulled-out of the matrix.

- The nanotubes should be well dispersed. If they are poorly dispersed, the nanotubes will fail by separation of the bundle rather than by failure of the nanotube itself, resulting in significantly reduced strength [111].

A theoretical estimate of the maximum tensile strength of the composites, valid for long aligned fibers, is provided by [113]

$$\sigma_{composite} = \sigma_{\mathrm{CNT}}\,\phi_{\mathrm{CNT}} + \sigma_m \phi_m, \qquad (7)$$

where $\sigma_{composite}$, σ_{CNT} and σ_m are the tensile strengths of the composite, CNTs and polymer matrix, respectively, and ϕ is the volume fraction. For example 5 wt% SWCNTs in PI: ϕ_{CNT} = 3.3 vol%, σ(SWCNT) ≈ 30 GPa [13] and σ_{PI} = 1 MPa (**paper III**), give $\sigma_{composite}$ ≈1 GPa, whereas the experiment yielded ≈4.5 MPa.

There are several models for estimating the Young's modulus and one of the most commonly employed is the Halpin-Tsai model, which exists in various forms. In the case of unixially aligned fibers, or CNTs it is given by [114]

$$\frac{E_{composite}}{E_m} = \frac{3}{8}\left[\frac{1+2p\eta_L\phi}{1-\eta_L\phi}\right] + \frac{5}{8}\left[\frac{1+2\eta_T\phi}{1-\eta_T\phi}\right], \qquad (8a)$$

where

$$\eta_L = \frac{E_{\mathrm{CNT}}/E_m - 1}{E_{\mathrm{CNT}}/E_m + 2p},$$

and

$$\eta_T = \frac{E_{\mathrm{CNT}}/E_m - 1}{E_{\mathrm{CNT}}/E_m + 2},$$

where E_{CNT} and E_m are the Young's moduli of the CNTs and matrix, respectively, ϕ is the volume fraction, and p is the aspect ratio, i.e. the ratio between the CNT's length and diameter. This equation should give an upper limit of Young's modulus and for a polyisoprene composite with 5 wt% SWCNTs it gives $E_{composite}$= 64 MPa, which is higher than the experimental value of E=27 MPa (see **paper III**).

When the fibers, or CNTs, are dispersed by solution mixing using an ultrasonic probe, which was employed in this work, these appear to become randomly oriented in three dimensions. In this case, the Halpin-Tsai model, the composite modulus $E_{composite}$ is given by [114]

$$\frac{E_{composite}}{E_m} = \frac{1}{5}\left[\frac{1+2p\eta_L\phi}{1-\eta_L\phi}\right] + \frac{4}{5}\left[\frac{1+2\eta_T\phi}{1-\eta_T\phi}\right]. \qquad (8b)$$

In this case, a 5 wt% polyisoprene-SWCNT composite gives $E_{composite}$= 36 MPa.

Moreover, by adding of 5 wt% SWCNTs (with aspect ratio ~380) in PE, the Young's modulus predicted by the Halpin-Tsai model is 16 GPa (assuming E_{SWCNT}= 1 TPa) [115], whereas experiment showed that E improve from 0.65 to 1.25 GPa, i.e. much less than the theoretically predicted value. At higher CNTs loading, the extent of improvement in mechanical properties might be limited by the high viscosity of the composite and the resulting void defect [105].

One can conclude that the Young's modulus and strength of polymer-nantoubes composites should increase with nanotube loading, dispersion and alignment in the matrix, but this assumes that the interfacial contact is sufficient so that the failure is not due to CNTs pull out. The large differences between the theoretical estimates and the experimental results might thus be caused by insufficient interfacial contact.

2.3.2.2 Thermal properties

The high thermal conductivity κ of CNTs (section 2.1.4.2) has led to expectations that CNTs can enhance much κ of polymer nanocomposites. But the progress in promoting κ has been less successful than that for electrical conductivity. This can be due to several reasons. One is that the relative difference in κ between CNTs and polymers is much less than the corresponding difference in electrical conductivity. The ratio ($\kappa_{CNT}/\kappa_{polymer}$) is 10^4 whereas the corresponding ratio of the electrical conductivity can be as large as is 10^{15}-10^{19} [110]. This means that the properties of the matrix will be more important for achieving high κ in a polymer composite. In the case of electrical conductivity, the electrons can (will) move through the composites via highly conducting CNTs. Moreover, the heat is transported by lattice waves and the stiff CNTs support entirely different (high frequency) waves than the soft polymer. It means that high frequency lattice waves of CNTs must be converted to low-frequency lattice waves at the boundary to the polymer matrix, and vice versa. The much too high predicted values for κ of polymer CNT composites as compared to experimental ones have been attributed due to a large interfacial thermal resistance between the matrix and the CNTs [116]. Although these difficulties can be obstacles for obtaining very high κ, it is also important to consider the amount of CNTs, SWCNTs or MWCNTs, the diameter and length, as well as their orientation in the polymer matrix, for optimizing κ.

For a theoretical estimate of κ for the composites one can use a model which can account for interfacial thermal resistance between the CNTs and the polymer. In this model, κ of a SWCNTs polymer composite, κ_{eff}, is given by [117]

$$\frac{\kappa_{eff}}{\kappa_m} = 1 + \frac{\phi p}{3} \frac{\kappa_{CNT}/\kappa_m}{p + \frac{2a_\kappa}{d}\frac{\kappa_{CNT}}{\kappa_m}}, \qquad (9)$$

where p is the aspect ratio, i.e. the ratio between the CNT length L and the CNT diameter d, κ_{CNT} and κ_m are the thermal conductivity of CNTs and matrix, respectively, and ϕ is the volume fraction of CNTs, and a_κ is a so-called Kapitza radius. It is defined by

$$a_\kappa = R_\kappa \kappa_m \ , \qquad (10)$$

where R_K is the interfacial thermal resistance across the carbon nanotube matrix. That is, R_K = 0 corresponds to perfect thermal contact between the CNTs and the polymer. R_K has been estimated as $R_K \sim 8\times10^{-8}$ m^{-2} K W^{-1} [116].

Among the best improvements observed is that by Haggenmueller *et al.* [118], who reported a 600% increase of κ by adding 20 vol% SWCNTs in high density polyethylene. Moreover, the increase was larger than predicted by a linear extrapolation from results at low CNT content, which indicates a percolation effect, i.e. that the heat is conducted through the composite via a network of the highly thermally conducting CNTs. Furthermore, Biercuk *et al.* [119] reported a 125% increase in κ of an epoxy at room temperature by loading 1 wt% raw laser-oven SWCNTs.

In addition to improving κ, the incorporation of CNTs commonly also increases the glass transition, melting and thermal decomposition temperatures of the polymer matrix due to their constraining effects on the polymer segments and chains. This is an important effect as it improves the thermal endurance of the polymer composites. For example, by adding 1 wt% CNTs to epoxy, the glass transition temperature increased from 63 to 88 °C [120] and, similarly, by adding 1 wt% SWCNTs to poly(methyl methacrylate) (PMMA) the glass transition temperature increase by ~40 °C [121].

Polymers typically have an intrinsic thermal conductivity, which normally is significantly lower than those of metals and ceramic materials. In many applications which require high thermal conductivity, such as electronic packaging and encapsulations, printed circuit boards, connectors, satellite devices, and in other areas where good heat dissipation, low thermal expansion and light weight are need, polymers reinforced with filler, organic or inorganic, are becoming more and more common. In these cases, the advanced polymer CNT composites may become useful with their good thermal conductivity, high thermal stability and low weight.

3. EXPERIMENTAL METHODS

3.1 The Transient Hot-Wire Method

In this thesis several experimental techniques are presented including the transient hot-wire method, which was to study the thermal conductivity κ and heat capacity per unit volume ρc_p of the pure polymers and their carbon nanotube composites. The method has been described in detail by Håkansson [122].

The transient hot-wire method probe was a nickel (Ni) wire. Nickel has an electrical resistance that depends strongly on temperature, which makes it well suited for hot-wire experiments. Moreover, nickel has a high tensile strength which makes it suitable to use in a high pressure environment. The hot-wire probe is installed horizontally and the wire is surrounded by the sample under investigation for which κ and ρc_p are to be determined.

During measurements, an electrical current is passed through the nickel wire by a short pulse of a few seconds, and the temperature rise of the wire is determined as a function of time. That is, the wire works as both heater and sensor for the temperature rise, which is calculated from the measured data of the wire resistance during the heating event using a predetermined calibration function. The temperature increase depends on the supplied energy and the thermophysical properties of the wire and surrounding sample. As described further below, an analytical solution of the time-dependent Fourier equation for heat conduction is fitted to the data for the temperature rise thereby yielding κ and ρc_p of the sample.

3.1.1 Theory

The measurement of κ and ρc_p by the transient hot-wire method is based on a solution of the Fourier equation,

$$\frac{\partial^2 T}{\partial r^2} + \frac{1}{r}\frac{\partial T}{\partial r} - \frac{\rho c_p}{\kappa}\frac{\partial T}{\partial t} = 0, \qquad (11)$$

where T is the temperature, t is the time and r is the radial co-ordinate, respectively.

To solve this equation, a few approximations is made: (i) the Ni-wire is assumed to be a perfect thermal conductor, (ii) at $t \geq 0$ the Ni-wire is assumed that to be heated by a uniform power q per unit length of the wire, (iii) the thermal contact resistance between the Ni-wire and the sample is neglected, and (iv) the Ni-wire is immersed in an infinitely large sample of infinite

length. The solution of the temperature rise of the Ni-wire is then given by Carslaw and Jaeger [123]

$$\Delta T = \frac{2q\alpha^2}{\pi^3\kappa} \times \int_0^\infty \frac{1-\exp(-\beta u^2)}{u^3\left\{\left[uJ_0(u)-\alpha J_1(u)\right]^2+\left[uY_0(u)-\alpha Y_1(u)\right]^2\right\}}du \ , \qquad (12)$$

where $\alpha = \frac{2\rho c_p}{\rho_{wire}c_{wire}}$ and $\beta = \frac{\kappa t}{\rho c_p r^2}$,

where ρ_{wire} and c_{wire} are the density and specific heat capacity of the Ni-wire, J_o and J_1 are Bessel functions of the first kind of zero and first order, and Y_o and Y_1 are Bessel functions of the second kind of zero and first order. This equation is fitted to the measured values for the temperature rise of the Ni-wire, using κ and ρc_p of the sample as fitting parameters, thereby yielding both κ and ρc_p.

3.1.2 Experimental

The hot-wire probe is typically approximately 40 mm in length with a diameter of 0.1 mm (or 0.3 mm). This length has been shown sufficient to fulfill the length requirement (iv) without introducing a large error [122]. The probe wire is placed horizontally in a ring of constant radius within a Teflon measurement cell as shown in **figure 13**a. The cell arrangement has been described in detail previously [124]. The distance to the cell wall of about 5-10 mm is large enough to fulfill the sample size requirement (iv) for the samples studied here. The probe is connected with four copper wires, where two are for current supply and the other two for voltage measurements. The hot-wire probe is immersed in the medium of investigation. In the case the sample is a liquid, it is simply poured into the cell. For a solid sample, two plates are made and one is placed below the wire and the other above. The (absolute) temperature of the sample is measured using an internal thermocouple (Chromel Alumel) which had been calibrated against a commercial calibrated diode sensor with an accuracy of 10 mK.

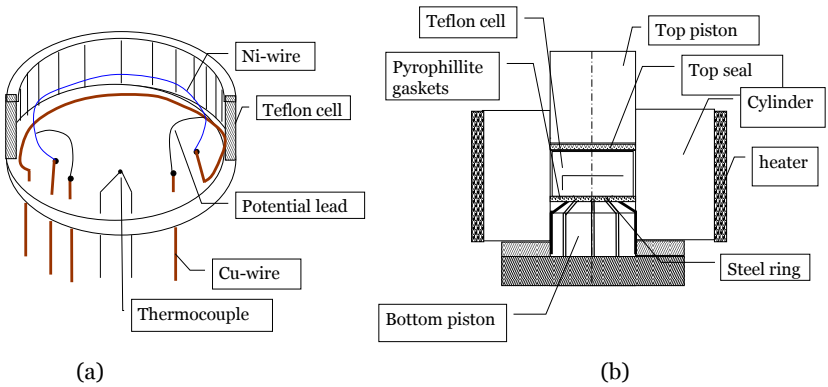

Figure 13. (a) The Teflon cell with hot-wire (Ni-wire) probe and thermocouple [124], (b) the high pressure equipment

The Teflon cell is sealed with a Teflon lid, and placed in a piston-cylinder type of pressure vessel with a 45 mm internal diameter, as shown in **figure 13**b and **figure 14**a. The whole assembly is transferred to a hydraulic press (see **figure 14**b) where load is applied. Our measurements are done at high pressure for three reasons: (i) to get good thermal contact between the hot wire and sample, (ii) to investigate the density dependence of thermal properties, [125] and (iii) to modify the microstructure of the samples, e.g. by cross-linking or changing the crystallinity. The pressure of the vessel is determined from load/area with an empirical correction for the friction which had been established using the pressure dependence of the resistance of a Manganin wire. The load is applied using a hydraulic press and two different types were used in this investigation. The maximum pressures of the set-ups were about 1 and 2 GPa, which were limited by the pressure cylinders. The maximum inaccuracy in pressure was approximately ±40 MPa at 1 GPa.

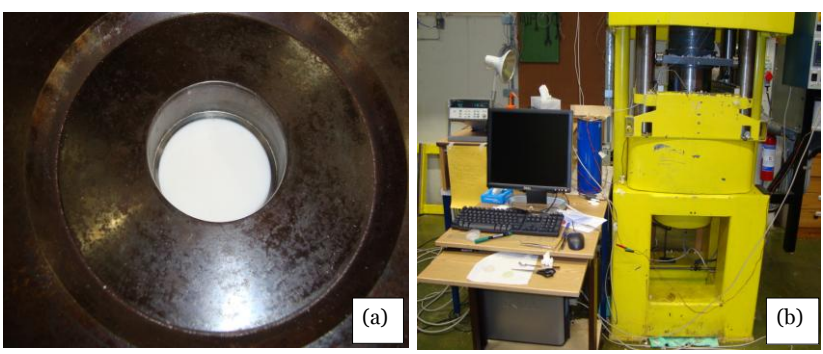

Figure 14. (a) High pressure cylinder with the Teflon cell lid (white) and top seal shown in the center, and (b) the yellow press, which was used most of the high pressure measurements.

For measurement above room temperature the temperature of the vessel was controlled by an external electrical power source by way of an electrical resistance coil heater, which was placed on the vessel. Both temperature and pressure were regulated using PID-controlled system. The PID controller maintained the temperature at a constant to within ±0.5 K during isothermal measurements above room temperature, and the pressure fluctuation was less than ±1 MPa during isobaric measurements. For measurements below room temperature, the vessel was cooled using liquid nitrogen.

3.1.3 Electronics and other details of the measurements

The electronic circuit for the hot-wire method measurement is shown in **figure 15**. The electronic circuit has a selective range for both heating current and pulse time, where the size of the current is selected by setting (eight) relays. This enables adjustment of the power to obtain a temperature rise of the Ni wire of about 4 K, which is considered to be an optimum value [122]. The measurement circuit is controlled by a PC coupled to a digital output card. The four wires of the hot-wire probe is connected to the electronic circuit as shown in **figure 15**. The hot-wire resistance R is thus in series with a Manganin resistance with a known predetermined resistance R_m. The measurements starts by a trigger signal sent from the digital output card to the clock in the circuit. The clock delivers simultaneously two signals: (i) a pulse (P **in figure 15**) which maintains an approximately constant voltage over the Ni wire and the Manganin wire, which in series with the Ni wire (when P is high, no current flows through the Ni wire), and (ii) 29 pulses which each simultaneously triggers two voltmeter set to measure the voltage over the Ni wire and the Manganin wire. When a constant voltage is applied to the wire, the power dissipates along the wire and causes a temperature change, which increases the electrical resistance of the wire. Since the resistance of the Manganin wire is temperature independent, the measurements of the Maganin voltages give the current through the Ni-wire. Thus, through the simultaneously measured Ni-wire voltages, the Ni-wire resistances during the heating event are obtained together with the dissipated power. In total, the heating event gives 29 resistances of the Ni-wire ($R_1 \ldots R_{29}$), which pertain to (known) increasing times t from the beginning of the heating event ($t_1 \ldots t_{29}$).

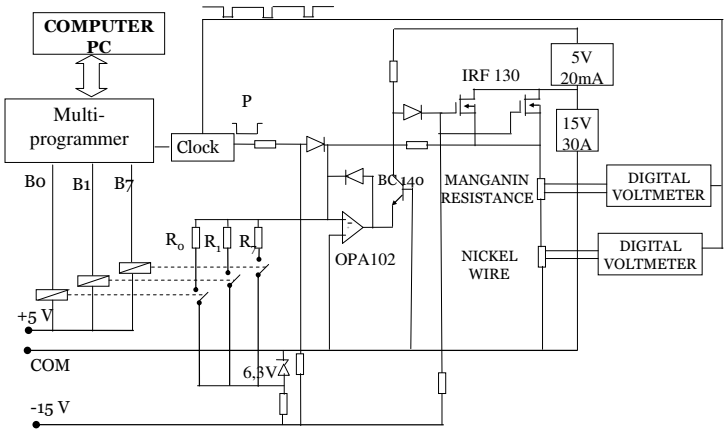

Figure 15. The measurement circuit [122].

3.1.4 Details of the calculation procedure

The length of the Ni wire between the potential leads l_0 and the radius of the Ni wire r_0, belonging to each heating event, needs to be determined since these values enter into the expression for the power per unit length and the expression for β in equation (12). The initial value for the length l_{00} was determined by a workshop microscope, and the initial radius r_{00} was calculated from the measurement of the weight of the wire using a literature value of the density of nickel at room temperature and atmospheric pressure. The values at any pressure and temperature were calculated using the compressibility and thermal expansivity of Ni together with the assumption that the resistivity and volume of the Ni-wire do not change during any plastic deformations, as described in more detail by Håkansson [122].

The measured resistances of the Ni wire during the heating event ($R_1 \ldots R_{29}$) must be transformed to temperatures ($T_1 \ldots T_{29}$), which is done through the calibration function, i.e. the known variation of the resistance of the Ni wire with temperature. The calibration results can be written in terms of a function as:

$$R(T) = R_s \, f(T), \qquad (13)$$

where R_s is the Ni resistance at a temperature T_s, and $f(T)$ is a function of temperature. The temperatures ($T_1 \ldots T_{29}$) can now be rewritten in terms of the resistance of the wire R_0 before the heating event at temperature T_0 as:

$$\frac{R_i}{R_0} = \frac{f(T_i)}{f(T_0)}. \qquad (14)$$

Rearranging of this equation gives the temperatures T_i of the Ni-wire during the heating event as:

$$T_i = f^{-1}\left[R_i\, f(T_0)/R_0\right], \qquad (15)$$

where i = 1...29.

Thus, the temperatures T_i can be calculated when R_0 is known. In order to obtain R_0, one uses an iterative method as follows:

a. Plausible estimates for κ and ρc_p of the sample (first values guessed) are inserted in equation (12) to yield an approximate ΔT_1, where ΔT_1 is the temperature increase of the Ni wire at time t_1, which yields an approximate T_1 from $T_1 = T_0 + \Delta T_1$

b. Through equation (14), with $T_1 = T_0 + \Delta T_1$, R_0 is calculated (R_1 and T_0 are obtained in the measurement).

c. Equation (15) is used to calculate the temperatures ($T_2 \ldots T_{29}$) from the measurement result of resistances ($R_2 \ldots R_{29}$).

d. Nonlinear fitting of equation (12) to the set of data ($t_0 \ldots t_{29}$), ($T_0 \ldots T_{29}$), with κ and ρc_p as adjustable parameters, yields better values for κ and ρc_p, which are used to repeat the sequence a to d.

The sequence a to d is repeated until the changes in κ and ρc_p are less than two predetermined values (0.1 % in κ and 0.5 % in ρc_p).

To avoid the time-consuming calculation of the integral in equation (12), values for ΔT, calculated using equation (12), are stored in a two-dimensional table of κ and ρc_p. In the nonlinear fitting procedure (step d), values for ΔT are thus obtained by interpolation in two dimensions instead of direct calculations using equation (12).

3.2 High Pressure Treatment

In this thesis work, a suitable high-pressure high-temperature technique to cross-link polymers and, in particular, polyisoprene and polybutadiene was established. The high temperature and high pressure treatments were performed in hydraulic presses of 1 GPa (yellow press **figure 14**b) and 2.5 GPa (blue press **figure 16**a) capacity. Samples of pure polymer or polymer-CNTs composite were loaded into Teflon cells, which fit in a 45 mm internal diameter piston-cylinder and transferred to a hydraulic press. The samples were pressurized at room temperature with a rate ~0.5 GPa h^{-1} from atmospheric pressure up to a pressure in the range 0.25 to 1.5 GPa. The pressure settings were determined from the applied force of the hydraulic press and the cross-sectional area of the piston with an empirical correction for friction, which was established using pressure dependence of a Manganin wire.

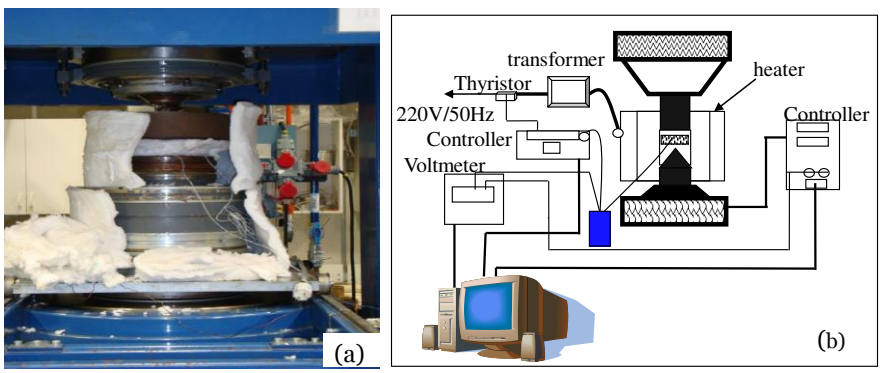

Figure 16. (a) The blue press and cylinder with 2.5 GPa capacity, and (b) schematic drawing of the temperature and pressure control system.

Subsequently, the samples were heated at a rate of 0.5 K/min isobaric from room temperature to ~500 K by means of an external heater that surrounded the vessel, and annealed for 4 h at 500 K. The temperature and pressure were controlled by PID-controller (see **figure 16**b); the pressure fluctuation during isobaric measurements was less than ± 1 MPa and the temperature sometimes fluctuated about ± 1 K during the 4 h anneal. The temperature of the sample was measured using an internal Chromel Alumel thermocouple with an estimated inaccuracy of ~0.2 K. The temperature gradient in the samples probably exceeded this during the cross-link process. In one experiment, the temperature gradient between the sample and the bottom of the Teflon cell (5 mm thickness) was established to ~7 K during

the annealing procedure. After annealing, the temperature was first decreased and the pressure lowered to atmospheric pressure and the samples removed from the cell. In order to obtain structural and mechanical properties, and the cross-linking density, the recovered samples were analyzed by the techniques described in the following sections.

3.3 Analytical Techniques

3.3.1 Fourier transform infrared spectroscopy

Basic principle

Fourier Transform Infrared spectroscopy (FTIR) studies concern the infrared radiation range (just above visible light in wavelength). Such radiation is sent from a source through the sample. The absorption is analyzed and provides information about the molecules since the absorption depends on their structure. A molecule can only absorb radiation when it is of the same frequency as one of the fundamental modes of vibration of the molecule, but the vibration must also be infrared active (e.g. the dielectric dipole moment must change during the vibration). The number of such fundamental vibrations of the structure is obtained by analyzing the degrees of freedom which the structure possesses. The resonance frequencies of the modes are dependent on the length of the bonds, and the masses of the atoms. That is, atoms in a molecule can vibrate only at certain specific frequencies that are limited and dependent on the neighbors and the type of bonding. For example, the most common unit in a polymer, the CH_2 group, can vibrate in six different ways, symmetrical and asymmetrical stretching, scissoring, rocking, wagging, and twisting, and some of these may cause detectable absorption at their fundamental frequency. FTIR is therefore a useful technique to study changes in a sample caused by the high pressure high temperature treatment used in this work.

The basic principle of recording the infrared spectrum of a sample is simplest described by the (old) dispersive technique. In such an instrument, a beam of *monochromatic* infrared light, which is obtained by a prism or grating, is passed through the sample and the amount of light absorbed by the sample is recorded as a function of wavelength. However, this is a slow method and also less accurate than a FTIR instrument.

The experimental set up

In a FTIR spectrometer a source provide a beam of infrared light, like in the old dispersive technique, but no prism or grating is placed in the path of the beam. That is, a beam consisting of the full spectrum of infrared frequencies is supplied to the sample for simultaneous measurements of their

absorbance. In order to derive the absorbance at each frequency one uses a set-up with an interferometer to obtain an interferogram, which is later deconvoluted to yield the desired absorbance vs. frequency data.

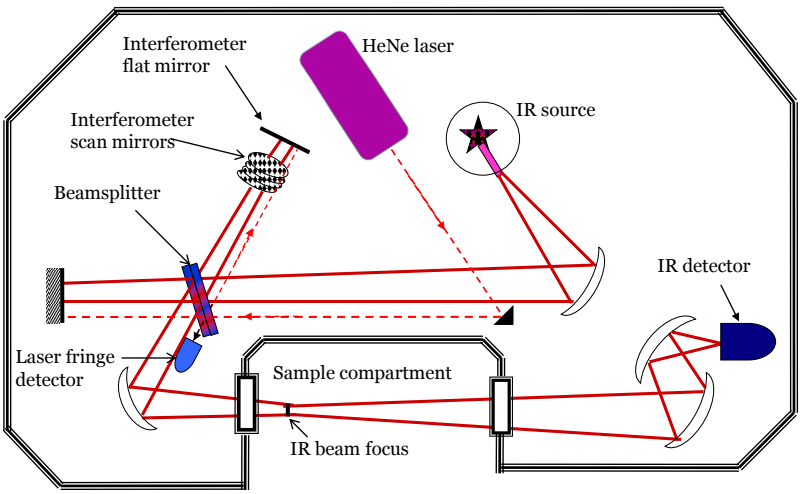

Figure 17. Optical path setup of the Perkin- Elmer II FTIR used in this thesis work [126]

A schematic view of the optical path of the FTIR (Perkin-Elmer II) spectrometer is presented in **figure 17**. The infrared beam begins at the source coil and is directed by a concave mirror towards a beam splitter, which splits the beam in two beams of equal intensity. One beam is reflected against a fixed flat mirror and the other against a movable flat mirror. The latter is placed on a mechanism which allows the mirror to move a very short distance, typically a few millimeters, away from the beam-splitter. Thus, the optical path for one of the two beams can be varied by moving the mirror, whose position is very accurately determined by a HeNe laser. The two beams are thereafter combined and the signal, which is called interferogram, depends on the position of the moving mirror. Subsequently, the beam enters the sample compartment where it is transmitted through or reflected off the surface of the sample, dependent on the type of analysis being conducted. After the infrared beam has passed through the sample compartment, the intensity is detected and the frequencies are demodulated via a Fourier Transform, which yields a raw, or single beam, spectrum. The spectrum is a graph of the intensity at the detector versus frequency. It contains information not only about the full infrared spectrum of the sample absorption, but also about the whole instrument, including the source, the optical components, gases in the path, etc. Thus all information not related to the sample has to be removed from the raw spectrum, which is done by measurements of a reference spectrum, i.e. a spectrum without a sample. To summarize, the key difference between a FTIR and an old type of dispersive

instrument is the modulation of the signal by the moving mirror together with the later demodulation by Fourier transformation.

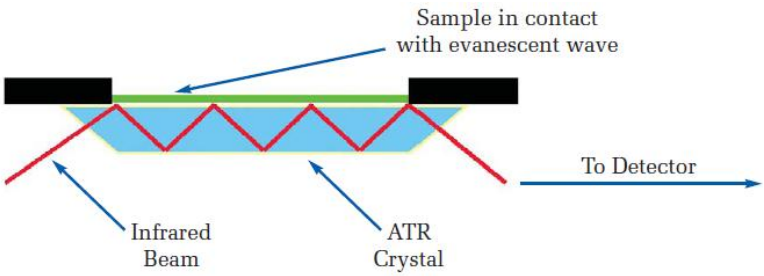

Figure 18. Principle of ATR.

In this work, we used Perkin-Elmer II FTIR with attenuated total reflectance (ATR) accessory. ATR is a very convenient method for studying solid samples since no sample preparation is needed. In this case, an ATR crystal, which in our case is a diamond, serves as a guide for the infrared beam that is reflected against the surface of the sample, as shown in **Figure 18**. Although the beam is reflected, it extends 0.5-5 μm into the sample where the sample molecules absorb the IR radiation characteristic of their vibrational modes. To reduce interference of carbon dioxide and water vapor, the sample compartment was filled with dry nitrogen gas. A background, or reference, scan (i.e. a scan without any samples) was done before a new sample was studied. The sample scan mode was set to determine the "percent transmittance" with respect to the background scan, i.e. 100% transmittance means that the sample scan gave the same intensity as that of the background scan. The spectra were taken in the wavenumber range 4400-600 cm^{-1}. Generally, the resolution and number of the scans for each measurement depended on the sample and were selected after a number of tests, but we typically used a resolution of 4 cm^{-1} and 16 scans.

3.3.2 Raman spectroscopy

Basis principle

Raman spectroscopy is based on inelastic scattering of monochromatic light, which is usually obtained from a laser source. When the laser light is incident on a sample, the photons interact with the electric dipoles of the sample molecules and become scattered. The majority of the scattered photons have the same frequency (energy) as the incident photons, i.e. these are elastically scattered, which is referred to as Rayleigh scattering. However, a small fraction of the scattered photons have different, and usually lower,

frequencies (energies) than the incident photons of the laser light. This inelastic scattering process is called the Raman effect. Raman scattering occurs due to a change in the vibrational, rotational or electronic energies of a molecules, and is illustrated schematically in **figure 19**. The laser light induces an oscillating dipole moment and excites the sample molecules into virtual energy states, from which the molecules de-excites through one of three possible processes, as shown in **figure 19**. In the elastic Rayleigh scattering, the excited molecule returns back to the same basic vibrational state and, therefore, the scattered photon has the same frequency as that of the excitation source. In the in-elastic Raman scattering there are two possibilities as the molecules can return to a higher or lower energy states, known as Stokes and anti-Stokes scattering, respectively. Consequently, Stokes and anti-Stokes spectra contain the same information, but the intensity of the latter is normally much weaker.

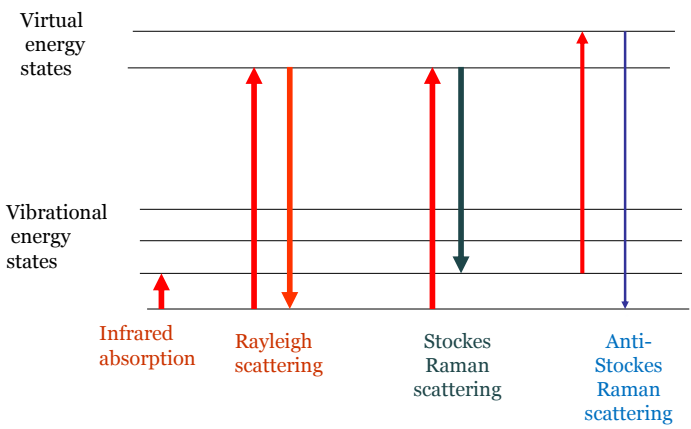

Figure 19. Raman transition schemes (the thickness of the lines indicates differences in the signal strengths).

Raman spectroscopy is commonly used in condensed matter, materials science, and chemistry. It provides a spectral fingerprint of substances and can be used to identify functional groups. That is, FTIR and Raman spectroscopy provide similar information. However, these can also provide complimentary information as the requirements for the processes are different, i.e. a Raman active mode may not be observed in FTIR and vice versa. Raman scattering requires that the polarizibility of the sample molecules changes during the vibration, whereas FTIR requires a change in the electric dipole moment. Moreover, as shown in **figure 19**, FTIR reflects a direct process between the energy states of the molecules. This is an advantage when the high-energy Raman source give rise to strong fluorescence and the Raman spectrum may therefore not be accessible.

The experimental set up

The optical path view of the Renishaw 1000 micro-Raman grating spectrometer with back scattering geometry at the Physics Department in Umeå is shown in **figure 20**.

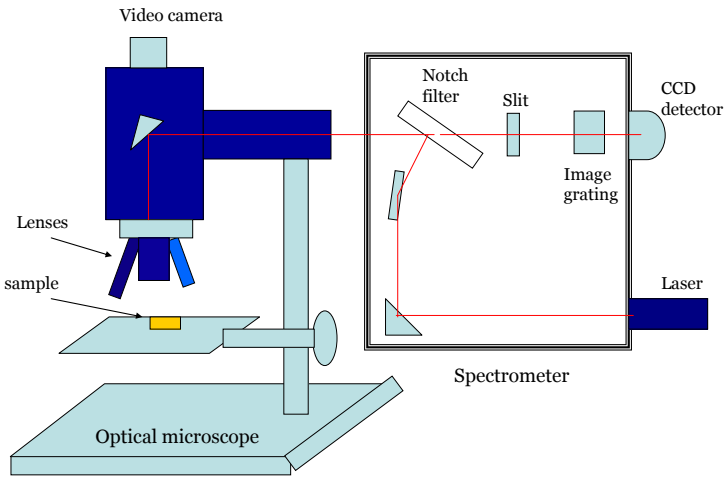

Figure 20. Raman spectrometer setup with an optical microscope adopted from Wågberg [127].

The video camera and micrometer are used for positioning of the laser spot on the sample. After interfering with the sample, the back-scattered light is directed back into the spectrometer, and a notch filter eliminates the Rayleigh light, i.e. the notch-filter cuts off the spectral range close to the laser line. This is necessary to avoid saturation of the Charge-Coupled Devices (CCD) detector by the high intensity elastically scattered light. The Raman-scattered light is passed through a slit onto a single grating and then registered by the CCD detector. In this way, the intensity of Raman-scattering light can be registered at each wavenumber separately. The spectrometer is equipped with four different lasers: a diode laser (deep red-IR, 780 nm), a HeNe laser (red, 632.5 nm), an Argon ion laser (Ar^+ ion, green, 514.5 nm), and a He-Cd laser (UV, 325 nm).

However, since the Raman spectra of the PI-CNTs composites studied in this thesis were often affected by fluorescence, the Raman results had limited use in the analysis of the composites.

3.3.3 Tensile tests

The mechanical properties of both pure polymers and polymer-CNTs composites treated under high pressure high temperature conditions were measured using an Instron 3343 with 500 N or 1 kN load cells at room temperature with a constant elongation speed of 10 mm/min until the specimen broke. The samples were cut from the high produced plates using a custom-made dogbone-shaped die (see **figure 21**a). The exact dimensions of the dogbone shaped samples were measured using a workshop microscope, but these were typically ~16 mm long, ~7 mm wide, and ~ 2 mm thick. At least two samples of the same type were tested. The tensile stress was calculated from load/initial cross section area, and values for the Young's modulus were obtained from stress/strain in the range of 1-5% strain, which typically was in the elastic regime.

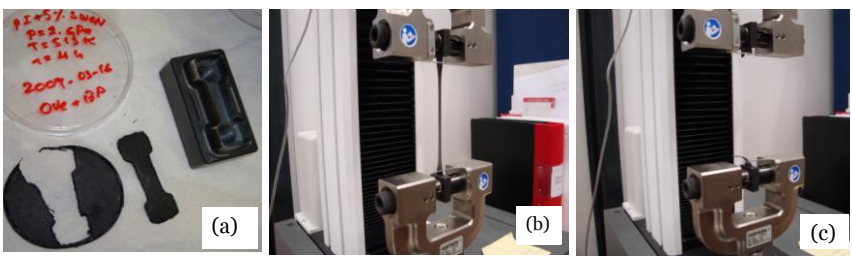

Figure 21 (a). Dogbone shaped sample and the custom-made die, (b) and (c) tensile testing using Instron 3343 before and after sample broke, respectively.

3.3.4 Swelling measurement

Swelling measurement is used to characterize rubber networks and it is based on a relationship between the molecular weight and the degree of swelling, which gives the cross-link density, as described in more detail in Ref. [128] and below. All samples were swelled at room temperature in either n-heptane or toluene. It was shown that swelling during several hours was enough to reach the equilibrium stage. At least three specimens from different places of the plates produced under high pressure were swelled. All samples were weighed, first before swelling, then in a swollen state after wiping off excess solvent, and finally after drying until the sample weight became constant (the mass of each piece of the sample was in the range 0.1-0.3 g). The crosslink density was then calculated using the Flory-Rehner equation [129,130]

$$\upsilon = -\frac{\ln(1-\phi_{NP}) + \nu_{NP} + \chi \nu_{NP}^2}{2V_s\left(\nu_{NP}^{1/3} - 2\nu_{NP}/f\right)}, \qquad (16)$$

where υ is the crosslink density (mol cm^{-3}), V_s is the molar volume of the solvent, f is the functionality of the crosslinking network, χ is the polymer-solvent interaction, and ϕ_{NP} is the volume fraction of the network polymer in the swollen sample, calculated as:

$$\phi_{NP} = \frac{(m_d - m_f)/\rho}{\left[(m_d - m_f)/\rho\right] + \left[(m_s - m_d)/\rho_s\right]}, \qquad (17)$$

where m_d is the mass of the sample after swelling and subsequent drying, m_s is the mass of the swollen sample, m_f is the mass of the filler in the sample, ρ is the polymer density and ρ_s is the density of the solvent.

3.3.5 Mass density

The mass densities of the samples were measured by either the Archimedes' principle by quickly immersing in water or by submerging the samples in mixtures of water and methanol of known density. A high-accuracy laboratory balance with an error of less than 0.1 mg was used to determine the mass of the sample. In the cases the sample had a lower density than water, a sinker was attached below the sample. The sinker was first submerged in water and the balance adjusted to 0 (zero) and then the sample was submerged. Special care was taken to avoid that the sample and the sinker touched the side of the beaker and that air bubbles were trapped on the surface of sample or the sinker. We then recorded the mass reading of the balance to obtain the volume of the sample.

3.3.6 Scanning probe microscopy

Basic principle

Scanning probe microscopy refers to techniques in which surface images are obtained by moving a probe back and forth over a sample, as described schematically in **figure 22**a. There are various types of scanning probe microscopy e.g. scanning tunneling microscopy (STM), scanning force microscopy (SFM) (also called Atomic Force Microscopy (AFM)). STM was the first in the scanning probe microscopy family. STM uses the exponential dependence of the tunneling current amplitude on the tip-sample distance to achieve sub-atomic resolution imaging. Thus, STM requires that the samples are conductive, but a few monolayers of an isolator can be studied if these are grown on a metal base. AFM is based on the force between the AFM tip

and sample surface, and can therefore be used to study any surface [131]. The AFM probe is a sharp tip mounted at the end of a cantilever and it is scanned above the sample to be studied. The cantilever behaves like a spring, and it is fixed at the opposite end of the mounted sharp tip. The tip is contacting the sample surface with nano-newton forces, or oscillating a few Angstroms above the sample. The AFM senses forces through changes in the cantilevel resonance frequency when it gently contacts the surface of the sample. Depending on the mode of operation it is referred to as contact or tapping mode.

The contact mode refers to the case when the tip contacts the surface through the adsorbed fluid layer on the sample surface. The tip operates in the repulsive regime of the tip-sample force, which is balanced by the elastic force of the cantilever pushing the tip downwards. The cantilever has low spring constant and is about 450 μm long with a tip diameter of less than 10 nm. A disadvantage of this method is that the tip and/or sample may be damaged by the contact and forces normal to the tip-sample interaction can be high due to capillary forces from the fluid sample surface layer.

Tapping mode is when the tip oscillates above the adsorbed fluid layer on the surface or when the tip lightly taps on the sample surface during scanning. The cantilever has a high spring constant, and is rather short. In this mode, very small forces are needed for scanning and there is less damage to soft samples i.e. biological samples, polymers, etc. However, tapping mode requires slower scan speed than contact mode.

In a typical AFM system, a laser beam is deflected from the back of the cantilever and recorded by a position photodiode detector. Constant amplitude (or frequency) of the cantilever oscillation is maintained by a feedback loop by maintaining a constant root mean square (RMS) of the oscillation signal acquired by the photodiode detector. The scanner moves up and down in z direction in order to maintain a constant set-point amplitude, and the vertical position of each (x, y) data point is stored by computer to form the topographic image of the sample.

The experimental set up

In this work, only the AFM tapping mode was used because of its suitability in studies of soft materials such as polymers and their carbon nanotube composites. The operational principle of the setup is described schematically in **figure 22**b.

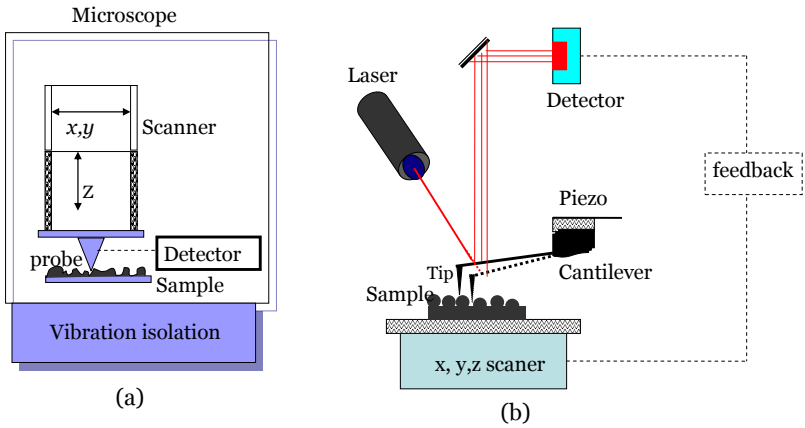

Figure 22: (a) Basic SPM components, (b) a diagram of a typical AFM set-up [132].

The AFM used here is from Veeco Metrology. A piezoelectric crystal is used for the movement of the tip across the sample surface. The tips used in this study were LTESP etched Silicon (Si) with a diameter of less than 10 nm. The cantilever, which is made from Si, had a thickness in the range 6.5-7.5 μm and was 225 μm in length, 38 μm wide, with a spring constant of 48 N/m and resonant frequency of 190 kHz.

The piezoelectric scanner can be selected depending on the size requirements of the scans. The maximum scanning area can be up to 125 μm×125 μm, but with the most precise scanner (the "E scanner"), the area is limited to just over 13 μm×13 μm ×5 μm in the *xyz*- direction, respectively. Moreover, the scanning rate of the AFM is in the range 0.1 to 30 Hz (line/s) and typically less than about 0.5 or 0.7 Hz, which means that an image with a resolution of 1024 lines×1024 points takes about 20-30 minutes.

3.3.7 Scanning electron microscope and transmission electron microscope

The scanning electron microscope (SEM) is very useful to characterize morphology and structure of nanomaterials and has therefore become a central tool for nanotechnology research. A SEM can produce high resolution images of a sample surface, and under beneficial conditions it can reveal details of about one to five nanometers in size. This instrument differs from all other conventional microscopes, using light or electrons, in forming its image progressively and not all at once. As illustrated in **figure 23**a, a very

fine beam of electrons with energies up to 30 keV is focused on the surface of the specimen in the microscope and scanned across it in a pattern of parallel lines. As the high energy electrons collide with the specimen atoms at or near the sample's surface, the interaction causes emission of secondary electrons, elastically backscattered electrons from the primary beam, and characteristic X-rays as electrons from outer shells drops to vacancies in inner shells, which are produced by the collisions. The secondary and back-scattered electrons give information about the sample's surface topography whereas the X-rays and backscattered electrons provide information about the elemental composition and their distribution. To avoid interference with the electron beam the whole system need to be in vacuum prior to measuring.

SEM micrographs have a large depth of field yielding a characteristic three-dimensional appearance useful for understanding the surface structure of the sample. A magnification of more than 500 000 times is possible. The spatial resolution of the SEM depends on the size of the electron spot and it is also limited by the size of the interaction volume. Since the SEM spot size and the interaction volume are larger than distances between atoms, it cannot image individual atoms as a transmission electron microscope (TEM). In this work, the SEM images were obtained using a Philips XL-30 microscope equipped with a field emission gun operating at an acceleration voltage typically between 3 and 30 kV, see **figure 24**.

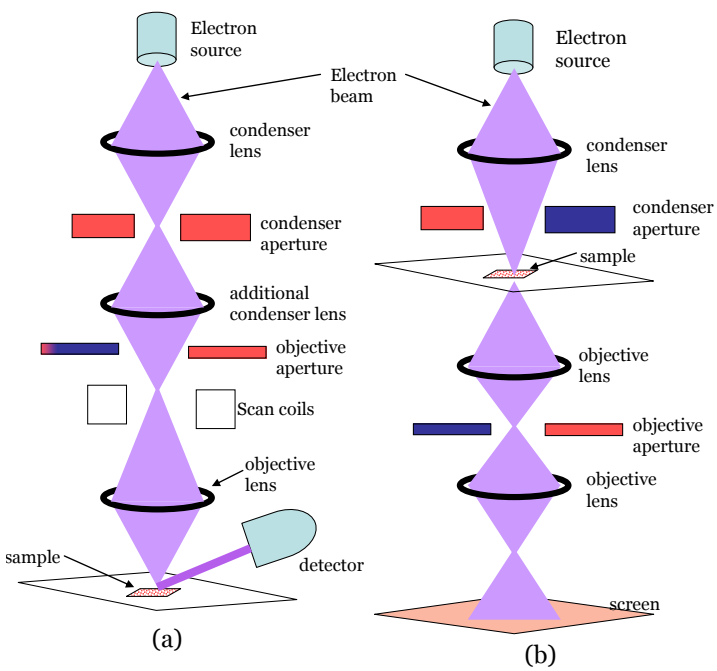

Figure 23. A sketch of the electron path in (a) a scanning electron microscope (SEM), and (b) a transmission electron microscope (TEM) [133,134]

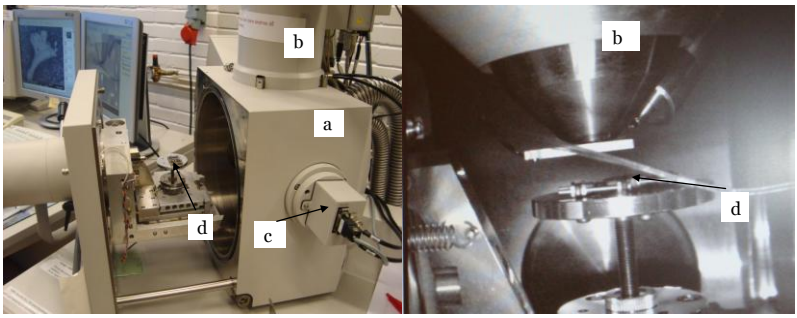

Figure 24. Pictures of a Philips XL-30 ESEM with respect different views and components: (a) vacuum cabinet, (b) electron gun, (c) detector, (d) samples.

The transmission electron microscope (TEM) is a derivative of the light microscope, which uses electron illumination instead of light and therefore achieves much better resolution. The basic principle of a TEM is shown in **figure 23**b. The whole system needs to be in vacuum to reduce electron scattering by gas molecules. The simplest TEM has two images lenses and is an exact analogy of the compound light microscope. The electron beam, which is ejected from an electron gun (emitted by a pin-shaped cathode, which is heated by a current) is focused on the sample by a condenser lens. The ejected electrons are accelerated by high voltage at the anode, which is in the range 50 and 200 kV, and then focused by a system of electronic coils (condenser) generating an electromagnetic field. After passing through the sample the electrons are focused by the objective lens into a magnified intermediate image and the final image is formed on a screen, a photographic film or a charge couple device (CCD) camera.

The resolution depends on the energy of the electrons (wavelength) and the quality of the sample preparation, as well as the components of the system, such as the electronic coils. Nowadays, the highest resolution realized is about 0.08 nm. Consequently, this instrument enables examination of individual atoms and crystalline defects. It is therefore an interesting instrument for evaluation and characterization of the morphology and structure of nanomaterials, but the requirement of very thin samples of a few 100 nm or less make the sample preparation difficult. The TEM used in this study is JEM-1230 (Jeol) equipped camera (Getan MSC 600W) and it was applied for imaging carbon nanotubes at 80 kV. The carbon nanotubes were dispersed in ethanol using sonication for 5 min and the well dispersed mixture was dropped on a copper grid and left for drying in the air.

4. SUMMARY OF THE INCLUDED PAPERS

In this section, I summarize the content of the papers which are included in this thesis, and I give a description of the extent of my contribution to each article.

Paper I

In this work, we investigated pure *cis*-1.4-poly(isoprene) PI with a number-average relative molecular mass of 38 000 g mol^{-1}. The results show that this polymer becomes cross-liked by high pressure and high temperature treatment without using any chemical cross-linking agents. The thermal conductivity κ and heat capacity per unit volume ρc_p were measured in both the virgin and cross-linked states in the range 160-513 K for pressure up to 0.75 GPa using the transient hot-wire method. We found that the results of κ and ρc_p were about the same at 295 K and 20 MPa for untreated and treated PI. Fourier transform infrared (FTIR) results before and after the treatment were in good agreement with literature results. Furthermore, it was found that PI exhibit two main relaxation processes and the effect of cross-linking and pressure on the behaviors of the processes were established.

I, together with my supervisor Dr. Andersson, performed the measurements by the hot-wire method under high pressure and high temperature (HP&HT) conditions. I performed swelling experiments and analysis after the HP&HT treatment. After many discussions of the results with my supervisor, I prepared the first version of the manuscript, including all figures.

Paper II

In this work, we investigated the thermal properties of polyisoprene single wall carbon nanotube (PI-SWCNTs) composites. The PI-SWCNT (1 and 5 wt%) composites were prepared by ultrasonic treatment of SWCNTs and PI in toluene. The measurements concerned the thermal conductivity κ and heat capacity per unit volume ρc_p for the PI-SWCNTs composites in the range 150-513 K and pressures up to 1 GPa both before and after HP&HT treatment. The κ of PI-SWCNT by 5 wt% composites loading at 0.02 GPa and 295 K, was found to be about 120% higher than that of pure PI, whereas the difference in κ between that before cross-linking (0.326 $Wm^{-1}K^{-1}$) and after (0.334 $Wm^{-1}K^{-1}$) was relatively small. Thus, the CNTs significantly increased κ, but these also caused a depression of the heat capacity per unit volume ρc_p of the PI matrix, which was a more surprising finding. The latter

was established by a discussion based on the mixture rule for ρc_p of PI-SWCNTs and the experimental results. The paper also provides the changes in glass transition temperature behavior caused by pressure and the HP&HT treatment. The measurements showed that the cross-linked composite had significantly higher glass transition temperature than the pure cross-linked polymer. Since the swelling measurements revealed that the composite, despite the same HP&HT treatment as the pure polymer, also attained much higher cross-link densities, this was believed to be the cause of the higher glass transition temperature. At the time of this work, we believed that the CNTs promoted chemical cross-linking but our later results (paper III) indicate the opposite and that the swelling results instead reflect physical cross-links/constraints caused by the CNTs and which is augmented by the HP&HT treatment. In the light of these later results, it should be these physical cross-links/constraints that also strongly raise the glass transition temperature in the cross-linked composite.

In paper II, transmission electron microscope imaging of the SWCNTs was carried out by Junchun Yu. I prepared the PI-SWCNTs composites and performed the thermal measurements of the PI-SWCNTs composite by the hot-wire method under HP&HT conditions. I also made the swelling measurements and prepared the first version of the manuscript. All three authors contributed to the evaluation of the results.

Paper III

This paper concerned mainly the mechanical properties of pure polyisprene (PI) and polyisoprene-single wall carbon nanotube composites (PI-SWCNTs) after high temperature and high pressure (HT&HP) treatments, which consisted of annealing for 4h at 513 K at pressures up to 1.5 GPa. We established both the effect of pressure treatment and CNT content on (ultimate) tensile strength (σ_{UTS}) and Young's modulus (E), and atomic force microscopy (AFM) phase images of the HP&HT treated samples showed that the CNTs were relatively well dispersed in PI. The shape of tensile curves showed that the polymer changes from elastomer towards brittle polymer with increasing treatment pressure, e.g. in the case of pure PI the σ_{UTS} improved by 650% and the E increased by 2000% between 1 and 1.5 GPa, simultaneously as the measured cross-linking density increased. We discuss the effect of CNTs on the properties after the HP&HT treatment and found that these seem to promote an increase of mass density and reduce the brittleness of the composites. An analysis based on scanning electron microscopy (SEM) images and literature results indicates that the CNTs-PI interaction gives physical cross-links/constraints, and swelling results imply that these increase with increasing treatment pressure. The simultaneous strong improvements of the mechanical properties made us conclude that cross-linking under high pressure can improve the interfacial interaction between CNTs and a polymer matrix.

In this work I prepared the PI-SWCNTs samples, I also carried out the HP&HT treatment, and the characterization by tensile testing, swelling and density measurements. AFM and SEM analyses were carried out by Junchun Yu and Britt Andersson. Finally, I prepared the first version of the manuscript.

Paper IV and V

These two papers deal with the properties of Nylon-6 and Nylon-6/MWCNTs composites before and after high pressure and high temperature treatments. The samples were studied by the transient hot-wire method, differential scanning calorimetry (DSC) and wide angle x-ray diffraction (WAXD). **Paper IV** establishes the glass transition temperature behavior of virgin nylon-6 based on results of the hot wire method and DSC. Moreover, a high pressure induced transition was detected and the changes in thermal properties, density, viscosity-average molecular weight, and microstructure (degree of crystallinity, crystal sizes and orientation) determined. **Paper V** deals with the properties of Nylon-6/MWCNTs composites produced by in-situ polymerization and subsequent pressure treatment. The paper reveals the effect of MWCNTs on the thermal properties and glass transition behavior, and we could show that despite a significantly increased degree crystallinity of the polymer matrix, the thermal conductivity of the composite remained largely unaffected.

I have participated in the preparation and carrying out of the HP&HT treatment, and taken part in the discussions of the manuscript.

Paper VI

This paper reports the thermal properties of liquid (PB2600) and solid (PB100000) polybutadiene with molecular weights 2600 and 100000 before and after HP&HT treatment at ~500 K and 1 or 1.5 GPa, which transformed the samples into densified (~20%) and well cross-linked ebonite-type of states. A Raman spectroscopy analysis showed that the HP&HT treatment caused significant changes of the Raman peaks. Most importantly, relatively strong and sharp Raman peaks due to the C=C vibrations in untreated PB2600, merged into one broad and weak peak, and a single peak due to the C=C vibration in untreated PB100000 almost vanished. This result shows that the carbon double bonds were consumed at the transformation. The transformation caused κ of PB2600 to increase by as much as 50% and ρc_p to decrease 15% at near ambient conditions compared to the untreated sample, and similar but somewhat smaller changes occurred for PB100000. Moreover the glass transitions of untreated PB2600 and PB100000

increased strongly on densification, which was described well by an empirical equation. The HP&HT treatment eliminated the glass transitions.

I have participated in the preparation and carrying out of the HP&HT treatment, and made all the thermal measurements on one of the polymers. I made an outline of the first version of the manuscript by compiling some of the results in figures, and I have been involved in the discussion of the results.

Paper VII

This work describes a comprehensive study of thermal and mictrostructural properties of PB2600 with up to 4.8 wt% SWCNTs, and PB100000 with up to 33 wt% MWCNTs. The results of the latter show remarkable changes in the mictrostructure after HP&HT treatment at ~500 K and 1.5 GPa. The initially well-dispersed CNTs appeared fused together into larger structures in a web-like pattern, and Raman results for the MWCNT's D* mode showed a large shift, indicating that the MWCNTs were subjected to significant stress. NMR data showed that ~50% of the double bonds were consumbed at the HP&HT induced transformation. Moreover, results before treatment showed that the glass transition temperature of the samples increased slightly compared to pure PB, and then more for SWCNT than MWCNTs and for the high molecular weight PB100000 under the most densified conditions.

I have participated in the preparation and carrying out of the HP&HT treatment. I have been involved in manuscript editing.

REFERENCES

[1] Agnieszka I-W, **studies of carbon nanomaterials based on fullerenes and carbon nanotubes**, PhD thesis, Umeå University**, 2007.**

[2] Nielsen, L. E.; Landel, R. F., **Mechanical propeties of polymers and composites**, 2nd ed., Macel Dekker, Inc. New York, **1994**.

[3] Moniruzzaman, M.; Winey, K. I., ***Macromolecules,* 2006**, *39*, 5194.

[4] Coleman, J. N.; Khan, U.;. Gun'ko, Y. K, ***Adv. Mater.*, 2006**, *18*, 689.

[5] Miyagawa, H.; Misra, M.; Mohanty, A. K., ***J. Nanosci. Nanotech.*, 2005**, 5(10), 1593.

[6] Kroto, H. W.; Heath, J. R.; O'Brien, S. C.; *et al.* ***Nature,* 1985**, 381, 162.

[7] Iijima, S., ***Nature,* 1991**, *354*, 56.

[8] Coleman, J. N.; Khan, U.; Blau, W. J.; Gun'ko, Y. K., ***Carbon,* 2006**, *44(9)*, 1624.

[9] Bokobza, L., ***Polymer*, 2007**, *48(17)*, 4907.

[10] Iijima, S.; Ichihashi, T., ***Nature,* 1993**, *363*, 603.

[11] Bethune, D. S.; Klang, C. H.; de Vries, M. S.; *et al.* ***Nature*, 1993**, *363*, 605.

[12] Dresselhaus, M. S., Dresselhaus, G., Avouris, Ph. **Carbon nanotubes synthesis, structure, properties, and Applications**, Spriger-Verlag Berlin Heidelberg, **2001.**

[13] O' Connell, M. J. **Carbon nanotube properties and applications**, CRS press, Inc., **2006.**

[14] Ebbesen, T. W. **Carbon nanotube: preparation and properties**, CRC press, Inc., **1997.**

[15] Meyyappan, M.; **Carbon nanotubes science and application**, CRC Press; Boca Raton, FL., **2005.**

[16] Harris, P. J. F.; **Carbon nanotubes and related structures new materials for the twenty-first century**, Cambridge University Press: Camridge, **2001.**

[17] Dresselhaus, M. S.; Dresselhaus, G.; Eklund, P. C.; **Scinece of Fullerenes and Carbon nanotubes**, Academic, New York, **1996.**

[18] Bacon, R., ***J. Appl. Phys.*, 1960**, *31*, 283.

[19] Endo, M.; Koyama, T.; Hishiyama, Y., ***Jap. J. Appl. Phys.*, 1976**, *15*, 2073.

[20] Oberlin, A.; Endo, M. ; Koyama, T., ***J. Cryst. Growth*, 1976**, *32*, 335.

[21] Oberlin, A.; Endo, M.; Koyama, T., ***Carbon,* 1976**, *14*(2), 133.

[22] Dresselhaus, M. S.; Dresselhaus, G.; Saito, R., ***Carbon,* 1995**, *33*, 883

[23] Odom, T. W. ; Huang, J. –L.; Kim, P.; Lieber, C. M., ***J. Phys. Chem. B,*** **2000**, *104*, 2794.

[24] http://nanopedia.case.edu/NWPage.php?page=nanotube.chirality

[25] Saito, R.; Dresselhaus, G.; Dresselhaus, M. S. ***Physical properties of Carbon Nanotubes***, **1998**, Imperial College Press (first published).

[26] Ajayan, P. M., ***Chem. Rev***., **1999**, *99*, 1787.

[27] Awasthi, K.; Srivastava, A.; Srivastava, O. N., ***J. Nanosci, Nanotechnol***., **2005**, *5,* 1616.

[28] Journet, C.; Maser, W. K.; Bernier, P.; *et al*., ***Nature,*** **1997**, *388*, 756.

[29] Thess, A.; Lee, R.; Nikolaev, P.; Dai, H. J.; *et al*., ***Science,*** **1996**, *273*, 483.

[30] Endo, M.; Takeuchi, K.; *et al*., ***J. Physical Chemistry Solids***, **1993**, *54,* 1841.

[31] Dai, H.; Rinzler, A. G.; Nikolaev, P.; *et al*., ***Chem. Phys. Lett.,*** **1996**, *260*, 471.

[32] Andrews, R.; Jacques, D.; Rao, A. M.; *et al*., ***Chem. Phys. Lett.***, **1999**, *303*, 467.

[33] Ducati, C.; Alexandrou, I.; Chhowalla, M.; *et al*., ***J. Appl. Phys***, **2002**, *92*, 3299.

[34] Kunadian, I.; Adrews, R.; Qian, D.; *et al*., ***Carbon***, **2009**, *47*, 384.

[35] Nikolaev, P.; Bronikowski, W. J.; *et al*., ***Chem. Phys. Lett***., **1999**, *313,* 91.

[36] Bronikowski, M. J.; Willis, P. A.; Colbert, D. T.; *et al*., ***J. Vac. Sci. Technol. A: Vacuum, surface, and films,*** **2001**, *19*, 1800.

[37] Zhou, W.; Ooi, Y. H.; Russo, R. ; *et al*., ***Chem. Phys. Lett***., **2001**, *350*(1-2), 6.

[38] Chattopadhyay, D.; Galeska, I.; Papadimitrakopoulos, F., ***Carbon,*** **2002**, *40*, 985.

[39] Bandow, S.; Rao, A. M.; Williams, K. A.; *et al*., ***J. Phys. Chem. B,*** **1997**, *101*(44), 8839.

[40] Shelimov, K. B.; Esenaliev, R. O.; *et al*., ***Chem. Phys. Lett***. **1998**, *282*, 429.

[41] Niyogi, S.; Hu, H.; Hamon, M. A.; *et al*., ***J. Am. Chem. Soc***., **2001**, *123*(4), 733.

[42] Zhao, B.; Hu, H.; Niyogi, S.; Itkis, M. E.; *et al*., ***J. Am. Chem. Soc***., **2001**, *123*, 11673.

[43] Reich, S.; Thomsen, C.; Maultzsch, J. **Carbon Nanotubes: Basic Concepts and Physical Properties**, Wiley-VCH, **2004**.

[44] Rotkin, S.V.; Subramoney, S. (Eds); **Applied Physics of Carbon Nanotubes. Fundamentals of Theory, Optics and Transport Devices**, Springer-Verlag, Berlin Heidelberg, **2005**.

[45] Loiseau, A.; Launois, P.; Petit, P.; Roche, S.; Salvetat, J.-P. (Eds); **Understanding Carbon Nanotubes. From Basics to Applications**, Springer-Verlag, Berlin Heidelberg, **2006**.

[46] Overney, G.; Zhong, W.; Tomanek, D.. ***Z. Phys. D: At., Mol. Clusters,*** **1993**, *27*, 93.

[47] Lu, J. P., ***Phys. Rev. Lett***., **1997**, *79*, 1297.

[48] Blakslee, O. L.; Proctor, D. G.; Seldin, E. J.; *et al.* T.**,** ***J. Appl. Phys***., **1970**, *41*, 3373.

[49] Frank, I. W.; Tanenbaum, D. M.; *et al.***,** ***J. Vac. Sci. Technol. B,*** **2007,** *25*, 2558.

[50] Van Enkevort, W. J. P., **Synthetic Diamond**; Spear, K. E.; Dismukes, J. P., Eds.; Wiley: New York, **1994**.

[51] Yu, M.F.; Files, B. S.; Arepalli, S.; *et al.,* ***Phys. Rev. Lett***., **2000**, *84*, 5552.

[52] Wong, E. W.; Sheehan, P. E.; Lieber, C. M., ***Science***, **1997**, *277(5334)* 1971.

[53] Lau, K. T.; Hui, D.; ***Composites Part B-Engineering***, **2002**, *33(4)*, 263.

[54] Vigolo, B.; Pénicaud, A.; Coulon, C.; *et al.*, ***Science,*** **2000**, *290*, 1331.

[55] Jiang, K.; Li, Q.; Fan, S., ***Nature***, **2002,** *419,* 801.

[56] Zhang, M.; Atkinson, K. R.; Baughman, R. H., ***Science***, **2004**, *306*, 1358.

[57] Dalton, A. B.; Collins, S.; Munoz, E.; *et al.*, ***Nature***, **2003**, *423*, 703.

[58] Gogotsi, Y., **Nantomaterials handbook**, CRC press Taylor &Francis group, **2006**.

[59] Berman, R., ***Phys. Rev***., **1949**, *76*, 315-316.

[60] Hone, J.; Batlogg, B.; Benes, Z.; *et al.*, ***Science,*** **2000**, *289*, 1730

[61] Yi, W.; Lu, L.; Zhang Dian-lin, Pan, Z. W.; *et al.*, ***Phys. Rev. B,*** **1999**, *59*(14), R9015.

[62] Wu, M. C. H.; Hsu, J. Y**.,** ***Nanotechnology***, **2009**, *20*(145401), 1.

[63] Hone, J.; Whitney, M., Zettl, A.*,* ***Synthetic metals***, **1999**, *103*, 2498.

[64] Hone, J., Whitney, M., Piskoti, Zettl, A., ***Phys. Rev. B,*** **1999**, *59*, R2514.

[65] Hone, J.; Llaguno M. C.; Briercuk M. J.; *et al.*, ***Appl. Phys. A***, **2002**, *74* , 339.

[66] Berber, S.; Kwon, Y. K.; Tománek, D., ***Phys. Rev. Lett***., **2000**, *84*, 4613.

[67] Kim, P.; Shi, L.; Majumdar, A.; *et al.*, ***Phys. Rev. Lett***., **2001**, *87*(21), 215502/1.

[68] Dresselhaus, M. S.; Dresselhaus, G.; *et al.*, ***Phil. Trans. R. Soc. Lond***. **A**, **2004**, *362*, 2065.

[69] Ando, Y.; Zhao, X.; Shimoyama, H.; *et al.,* ***Int. J. Inorg. Mater***., **1999**, *1*, 77.

[70] Andriotis, A. N.;Menon, M.;Chernozatonskii, L., ***Nano Lett***., **2003**. *3*(2). 131.

[71] Zhou, C.; Kong, J.; Dai, H., ***Phys. Rev. Lett***., **2000**, *84*(24) 5604.

[72] Dresselhaus, M. S.; Dresselhaus, G.; Saito, R.; *et al*., ***Phys. Rep***., **2005,** *409*, 47.

[73] Bandow, S., ***Phys. Rev. Lett***., **1998**, *80*, 3779.

[74] Alvares, L.; Righi, A.; Rols, S.; *et al*., ***Phys. Rev. B***, **2001**, *63*, 153401.

[75] Cooper, C. A.; Young, R. J.; Halsall, M., ***Comp. Part A***, **2001**, *32*, 401.

[76] Kwok, K.; Chiu, W. K. S., ***Carbon***, **2005**, *43*, 437.

[77] Nugent, M. J; Santhanam, K. S. V.; Rubio, A.; *et al*., ***Nano. Lett***., **2001**, *1*, 87.

[78] Lordi, V.; Yao, N.; Wei, J., ***Chem. Mater***., **2001**, *13*, 733.

[79] Niu, C.; Sichel, E. K.; Hoch, R.; *et al*., ***Appl. Phys. Lett***., **1997**. *70*(11), 1480.

[80] Lee, S. W.; Yabuuchi, N.;. Gallant, B. M.; *et al*., ***Nature Nanotechnology, 2010***, *5*, 531.

[81] Liu, T.; Sreekumar, T. V.; Kumar, S.; *et al*., ***Carbon,*** **2003**, *41*(12), 2440.

[82] Obreja V. V. N., ***Physica E***, **2008**, *40*, 2596.

[83] An, K. H.; Jeon, K. K.; Kim, W. S.; *et al*., ***J. Korean, Phys. Soc.,*** **2001**, *39*, S511.

[84] Wang, H. ; Qu, M.; Yu, Z. ; *et al*. ***Materials Chemistry and physics***, **2007**, *105*, 169.

[85] Pan, H.; Li, J.; Feng, Y. P., ***Nanoscale Res. Lett***., **2010**, *5*, 654.

[86] Du, C.; Pan, N., ***Nanotechnology***, **2006**, *17*, 5314.

[87] Roberts, A. D., **Natural rubber Science and Technology**; Oxford Univ. Press:Oxford, U.K., **1988**.

[88] Arjunan, V.; Subramanian, S.; Mohan, S., ***Spectrochimica Acta Part A***, **2001**, *57*, 247.

[89] Binder, J. L., ***J. Polym. Sci. Part A***, **1963**, *1(1),* 37.

[90] Cornell, S. W.; Koenig, J. L., ***Macromolecules,*** **1969**, *2(5)*, 546.

[91] Kohan, M. I., **Nylon plastics handbook**, New York, Hanser Gardner Pub.,**1995**.

[92] Gent, A. N.; Kaang, S. Y., ***J. Polym. Sci: part B: Polym. Phys***., **1989**, *27*, 893.

[93] Adachi, K., Kotaka, T., ***Macromolecules,*** **1988**, *21,* 157.

[94] Tobolsky, A. V.; Eisenberg, A., ***J. Am. Chem. Soc***., **1959**, *81*(4), 780.

[95] Breuer, O.; Sundararaj, U., ***Polym. Compos***., **2004**, *25*(6), 630.

[96] Jin, Z.; Sun, X.; Xu, G.; *et al*., ***Chem. Phys. Lett***., **2000**, *318*, 505.

[97] Peigney, A.; Laurent, Ch.; Flahaut, E.; *et al*., ***Carbon***, **2001**, *39*, 507.

[98] Schadler, L. S.; Giannaris, S. C.; Ajayan, P. M., ***Appl. Phys. Lett***., **1998**, *73*(26), 3842.

[99] Bryning, M. B.; Mikie, D. E.; *et al.*, ***Appl. Phys. Lett***., **2005**, *87*(16), 161909/1.

[100] Zhu, J.; Kim, J.; Peng, H.; *et al.*, ***Nano Lett***., **2003**, *3*, 1107.

[101] Gojny, F. H.; Schulte, K., ***Compos. Sci. Technol***., **2004**, *64*, 2303.

[102] Shen, J.; Huang, W.; Wu, L.; *et al.*, ***Compos. Sci. Technol***., **2007**, *67*, 3041.

[103] Ramanathan, T.; Fisher, F. T.; Ruoff, R. S.; *et al.*, ***Chem. Mater.***, **2005**, *17*, 1290.

[104] Ma, P. C.; Mo, S. Y.; Tang, B. Z.; *et al.*, ***Carbon***, **2010**, *48*, 1824.

[105] Zhu, J.; Peng, H.; Rodriguez-Macias, F.; *et al.*, ***Adv. Funct. Mater***., **2004**, *14*, 643.

[106] Frankland, S. J.V.; Caglar, A.; *et al.*, ***J. Phys. Chem. B***, **2002**, *106*, 3046.

[107] Kumar, S.; Dang, T. D.; Arnold, F. E.; *et al.*, ***Macromolecules,*** **2002**, *35*(24), 9039.

[108] Coleman, J. N.; Khan, U.; Gun'ko, Y. K., ***Adv. Mater.***, **2006**, 18, 689.

[109] Chae, H. G.; Sreekumar, T. V.; Uchida, T.; *et al.*, ***Polymer,*** **2005**, 46(24), 10925.

[110] Moniruzzaman, M.; Winey, K. I., ***Macromolecules,*** **2006**, 39(16), 5194.

[111] Schadler, L. S.; Giannaris, S. C.; Ajayan, P. M., ***Appl. Phys. Lett***., **1998**, *73*(26), 3842.

[112] Salvetat, J. –P.; Bonard, J. –M.; Thomson, N. H.; *et al.*, ***Appl. Phys. A***, **1999**, *69*, 255.

[113] Agarwal, B. D.; Broutman, L. G. **Analysis and Performance of Fiber Composites,** Wiley: New York, **1980.**

[114] Nielsen, L, E.; Landel, R. F., **Mechanical properties of polymer and composites**, Marcel Dekker, Inc, New York, **1994.**

[115] Haggenmueller, R.; Zhou, W.; *et al.*, ***J. Nanosci. Nanottechnol***., **2003**, *3*, 105.

[116**]** Huxtable, S. T.; Cahill, D. G.; Shenogin, S.; *et al.*, ***Nat. Mater***., **2003**, *2*, 731.

[117] Nan, C. W.; Liu, G.; Lin, Y. ; Li, M., ***Appl. Phys. Lett***., **2004**, *85*(16), 3549.

[118] Haggenmueller, R.; Guthy, C.; Lukes, J. R.; *et al.*, ***Macromolecules,*** **2007**, *40*, 2417.

[119] Biercuk, M. J.; Llaguno, M. C. ; *et al.*, ***Appl. Phys. Lett.***, **2002**, *80*(15), 2767.

[120] Gong, X. Y.; Liu, J.; Baskaran, S.; *et al.*, ***Chem. Mater.***, **2000**, *12*, 1049.

[121] Velasco-Santos, C.; Martínez-Hernández, A. L.; *et al.*, ***Chem. Mater***., **2003**, *15*, 4470.

[122] Håkansson, B.; Andersson, P.; Bäckström, G., ***Rev. Sci. Intruments,*** **1988**, *59*(10), 2269.

[123] Carslaw, H. S.; Jaeger, J. C. **Conduction of heat in solids**, 2nd ed. **1959** (Oxford University Press)

[124] Sandberg, O., **Thermal properties of Organic glass formers under pressure**, **1980** (Ph. D. thesis, Department of Physics, Umeå University, Umeå, Sweden,).

[125] Andersson, O., **Thermal conductivity and phase diagram of organic substances under pressure**, Doctoral thesis, Dep. of Physics, Umeå University, Sweden, 1991.

[126] **Spectrum BX, User's guide**, PerkinElmer Ltd, United Kingdom. 2005.

[127] Wågberg, T. **Studies of polymeric and intercalated phases of C_{60}**, *Doctoral thesis*, Dep. of Exp. Physics, Umeå University, Sweden, 2001.

[128] James E. M.; **Physical properties of polymer handbook**, **2007**, *Spriner Science+Business media, LLC*, 2nd ed.

[129] Flory P.J. Rehner Jr. J., ***J. Chem. Phys.,* 1943**, 11, 512.

[130] Flory P.J., ***J. Chem. Phys***., **1950**, 18, 108.

[131] Hofer, W. A.; Foster, A. S.; Shluger, A. L., ***Rev. Modern Phys***., **2003**, *75*, 1287.

[132] Bhushan, B.; Fuchs, H.; Hosaka, S., **Applied Scanning probe methods,** Springer-Verlag Berlin Heidelberg, **2004**.

[133] Stenmark, P., **Synthesis, modification and characterization of carbon nanostructures carbon nanotubes, fullerenes and fullerene derivatives**. Licentiate thesis in experimental physics performed at the department of Physics, Umeå University, Sweden, **2009**.

[134] Klinke, C., **Analysis of catalytic growth of carbon nanotubes**, PhD thesis, institut de physique des nanostructures section de physique, Fridericana University, **2003.**